Lipodystrophy can be uncoupled from detrimental metabolic consequences

Chandramohan Chitraju[1, 2], Alexander W. Fischer[1, 2, 7], Yohannes Abere Ambaw[1, 2, 3, 4], Kun Wang[1, 2], Bo Yuan[1], Sheng Hui[1], Tobias C. Walther[1, 2, 3, 4, 5, 6]* and Robert V. Farese, Jr.[1, 2, 5]*

[1]Department of Molecular Metabolism, Harvard T.H. Chan School of Public Health, Boston, MA 02115, USA

[2]Department of Cell Biology, Harvard Medical School, Boston, MA 02115, USA

[3]Center on the Causes and Prevention of Cardiovascular Disease (CAP-CVD), Harvard T.H. Chan School of Public Health, Boston, MA 02115, USA

[4]Harvard Chan Advanced Multi-omics Platform, Harvard T.H Chan School of Public Health, Boston, MA 02115, USA

[5]Broad Institute of Harvard and MIT, Cambridge, MA 02142, USA

[6]Howard Hughes Medical Institute, Boston, MA 02115, USA

*These authors contributed equally

[7]Present address: Moderna Therapeutics, Cambridge, MA 02139, USA

Correspondence should be addressed to:

Tobias C. Walther and Robert V. Farese, Jr.

Harvard T. H. Chan School of Public Health

Department of Molecular Metabolism

665 Huntington Avenue

Boston, MA 02115

twalther@hsph.harvard.edu and robert@hsph.harvard.edu

SUMMARY

Adipose tissue has at least two major functions: storing metabolic energy as triacylglycerols (TG) and coordinating metabolism by secreting hormones, such as leptin. In lipodystrophies, defects of storing TG are typically accompanied by metabolic abnormalities, such as hepatic steatosis, and endocrine perturbations. Thus, the concept emerged that the endocrine function of adipose tissue is coordinated with, and requires, TG stores. To test this notion, we selectively depleted adipose TG stores by deleting the TG synthesis enzymes, DGAT1 and DGAT2, in murine adipose tissue (ADGAT DKO mice). Despite markedly reduced TG storage, ADGAT DKO mice maintained ample adipose tissue endocrine function and surprisingly did not develop metabolic perturbations, even when fed a high-fat diet, owing to increased energy expenditure and beiging of white adipose tissue. These findings, thus, reveal that adipose tissue performs TG storage and endocrine functions largely independently from each other.

INTRODUCTION

Loss of white adipose tissue (WAT) leads to a condition known as lipodystrophy (Mann and Savage, 2019; Patni and Garg, 2015). Lipodystrophies can be congenital or acquired, and manifest as generalized or partial in adipose distribution and severity (Garg, 2004). Human mutations causing lipodystrophies are predominantly found in genes involved in adipose tissue development (e.g., *PPARG*) (Agostini et al., 2006; Hegele et al., 2002), glycerolipid synthesis (*AGPAT2*) (Agarwal et al., 2002), or lipid droplet formation (e.g., *BSCL2*, *PLIN1*) (Gandotra et al., 2011; Magre et al., 2001). Lipodystrophy patients nearly always present with many metabolic derangements, including ectopic lipid accumulation in the liver (hepatic steatosis), hypertriglyceridemia, and insulin resistance or diabetes (Lawrence, 1946; Misra and Garg, 2003; Reitman, 2002). A characteristic feature of lipodystrophy is the decrease in levels of adipose tissue-derived hormones, such as leptin (Friedman, 2019; Lim et al., 2021), and many derangements of lipodystrophies are corrected by leptin therapy (Oral et al., 2002; Shimomura et al., 1999). The discovery of leptin (Zhang et al., 1994) and its ability to correct these pathologies of lipodystrophy led to the concept that WAT is an endocrine organ (Kershaw and Flier, 2004; Scheja and Heeren, 2019).

Severe lipodystrophies are accompanied by large reductions in levels of triacylglycerols (TGs), the primary molecule for storing high amounts of metabolic energy, in WAT and often in the whole body. This reduction in fat mass, and TG energy storage, usually correlates well with decreases in leptin production from WAT and circulating leptin levels. Because of the tight correlation between adiposity and circulating leptin levels (Friedman, 2019), leptin has been assumed to monitor and report on adipose tissue TG stores.

Here, we sought to test the relationship of TG storage and endocrine adipose tissue function. We generated mice lacking both known TG synthesis enzymes, DGAT1 and DGAT2 (Cases et al., 1998; Cases et al., 2001), in adipose tissue. We expected to generate a mouse model of classic lipodystrophy due to defects of TG synthesis and storage in adipose tissue. Moreover, we hypothesized that these mice would have severe accumulations of TG in non-adipose tissues, such as the liver or skeletal muscle, resulting in lipotoxicity and metabolic derangements, such as insulin resistance or fatty liver disease. To our surprise, we found the opposite result. We report here that depleting TG stores in murine adipose tissue leads to a distinct form of lipodystrophy in which the endocrine function of WAT is largely intact and metabolic derangements are not observed. Remarkably, these mice are even protected from the adverse metabolic effects of a high-fat diet (HFD).

RESULTS

ADGAT DKO mice have reduced fat mass and triglycerides in adipose tissue

To generate mice lacking TGs in adipose tissue (ADGAT DKO), we crossed adipose tissue-specific *Dgat1* knockout mice (Cre-transgene expressed under control of the mouse adiponectin promoter (Eguchi et al., 2011)) with *Dgat2* flox mice (Chitraju et al., 2019). Validation of gene knockouts showed mRNA levels of *Dgat1* were decreased by ~95% and *Dgat2* by ~90% in both inguinal white adipose tissue (iWAT) and interscapular brown adipose tissue (BAT) (Figure S1A). Western blot analysis showed that DGAT1 and DGAT2 proteins were absent in iWAT and BAT (Figure S1B). *In vitro* DGAT activity in lysates of adipose tissue of ADGAT DKO mice was decreased by ~80% in iWAT and ~95% in BAT (Figure S1C).

ADGAT DKO mice appeared healthy (Figure 1A) and yielded offspring with the predicted Mendelian ratio of genotypes. Nuclear magnetic resonance imaging showed that fat depots were decreased in chow-fed ADGAT DKO mice (Figure 1B). Body weights of 12-week-old chow-fed control mice (*Dgat1* and *Dgat2* double-floxed mice, D1D2 flox) and ADGAT DKO mice were similar (Figure 1C), but dual-energy X-ray absorptiometry (DEXA) analysis revealed that the fat mass was decreased by ~60% in ADGAT DKO mice. The reduction in fat mass was persistent: DEXA analysis of 1-year-old ADGAT DKO mice showed that the fat mass was reduced by ~75% and that lean mass was increased by ~15% (Figure S1D). Visceral white adipose tissue depots (gonadal, mesenteric, pericardial, and perirenal fat depots) were markedly atrophied in ADGAT DKO mice (Figures 1D and S1E). Gonadal adipose tissue (gWAT) and subcutaneous inguinal WAT (iWAT) in ADGAT DKO mice appeared distinctly “beige” in color (Figures 1D and S1E). In ADGAT DKO mice, iWAT and BAT were denser, as demonstrated by their sinking in a liquid fixative (Figure 1F).

The interscapular BAT depot in ADGAT DKO mice appeared darker brown than that in control mice (Figure S2A). TGs and lipid droplets (LD) were undetectable in BAT of ADGAT DKO mice (Figures S2B and S2C). Positron emission tomography-computed tomography scanning using ^{18}-fluoro-deoxyglucose (^{18}-FDG-PET/CT) showed that, after injection of β-3-adrenoceptor agonist (CL 316,243), BAT of chow-fed ADGAT DKO mice took up more glucose than BAT of control mice (Figure S2D), presumably to fuel thermogenesis. In agreement with increased glucose uptake, glycogen levels in BAT of ADGAT DKO mice were increased in all conditions except 4°C cold exposure (Figure S2E). The latter condition may reflect increased glycogen requirements in BAT of ADGAT DKO mice to maintain thermogenesis. This phenotype of DGAT-deficient BAT exhibiting increased glucose uptake and glycogen stores as an alternate fuel is consistent with our previous findings of BAT-specific knockout of both DGAT enzymes (Chitraju et al., 2020).

ADGAT DKO mice activate an alternative mechanism to make triglycerides

DGAT1 and DGAT2 appear to account for most of TG synthesis in mice. Newborn mice lacking both DGAT enzymes have >95% reduction in whole body TGs (Stone et al., 2004), and adipocytes derived from fibroblasts lacking both enzymes fail to accumulate TGs or LDs (Harris et al., 2011). In agreement with this, histological analysis of WAT of 8-week-old ADGAT DKO mice showed fewer and much smaller LDs than control WAT (Figure 1E). However, by age 15 weeks, ADGAT DKO mice exhibited more LDs in iWAT than 8-week-old ADGAT DKO mice, suggesting that they activate alternate pathways to accumulate neutral lipids (Figure S3A). This finding was more prominent in iWAT than in BAT. The neutral lipid that accumulated was BODIPY-positive (Figure 1G), and TLC analysis of adipose tissue lipids from 15-week-old ADGAT DKO mice revealed the lipids to be TGs (Figure 1H). Feeding ADGAT DKO mice a HFD increased levels of TGs by ~twofold in iWAT at age 15 weeks, but the TG content of iWAT remained ~70% less than control mice (Figures S3A and S4A). The mass reduction of iWAT fat pads was accounted for predominantly by a decrease in TG mass per fat pad (Fig. 1I); protein levels per fat pad were similar to controls, and no other neutral lipids were detected. Lipid analyses of iWAT by mass spectrometry revealed that TG levels were reduced by ~80% across all detected TG species (Figures 1I and S3C). In contrast, several phospholipids were substantially increased in iWAT of ADGAT DKO mice (Figure 1I), which may have contributed to the residual fat mass of the iWAT fat pads. Enzyme assays revealed that adipose tissues from 15-week-old chow-diet-fed ADGAT DKO mice had detectable (~20% of normal) DGAT activity in iWAT that was not inhibited by DGAT1- or DGAT2-specific inhibitors (Figure S1C). These data suggest that deletion of DGAT1 and DGAT2 in WAT induces a DGAT activity from an alternative enzyme (Yen et al., 2005).

Adipose tissue TG stores are required to maintain activity and body temperature during fasting

Because ADGAT DKO mice have severely decreased TG stores, we expected that they would not tolerate fasting well. After 14 hours of fasting, 15-week-old ADGAT DKO mice had lost 10% of body weight (vs. control mice) (Figure 2A) and entered a torpor-like state with decreased physical activity and huddling together (Supplemental movie 1). Fasting of ADGAT DKO mice also resulted in hypothermia, with body temperatures dropping to ~30°C (Figure 2B), a phenotype exacerbated by cold exposure (Figures 2E and 2F). Fasting levels of ketone bodies were ~10% lower, and glucose levels were moderately higher in ADGAT DKO mice than control mice (Figures 2C and 2D), possibly reflecting their greater dependency on glucose as fuel. Thus, as expected, deletion of TG stores in adipose tissue resulted in reduced fuel stores that dramatically altered the physiological responses of the mice to fasting or cold.

Endocrine function of WAT is uncoupled from TG storage in ADGAT DKO mice

Lipodystrophy in humans and mice is accompanied by reduced levels of adipocyte-derived endocrine hormones and often results in insulin resistance and diabetes (Oral et al., 2002; Peterfy et al., 2001; Reue and Phan, 2006). However, despite the lack of TG storage in WAT of ADGAT DKO mice, adiponectin and leptin mRNA levels were moderately increased in iWAT (Figure 3A), whereas the mRNA levels of *Plin1* were unchanged (Figure 3A), and plasma levels of adiponectin and leptin were normal and 40% decreased, respectively, in these mice (Figure 3B). Although plasma leptin levels in ADGAT DKO mice were reduced, they were much higher than in control leptin-deficient *ob/ob* mice. Glucose levels in ADGAT DKO mice fasted for 4 h were slightly lower (169 ± 16 mg/dl vs. 144 ± 14 mg/dl, respectively, $p<0.01$) than in control mice, and insulin levels were not different (Figure 3C). Analysis of plasma metabolites showed a ~30% reduction in non-esterified fatty acids, a ~15% reduction in glycerol, and a ~50% reduction in ketones in chow-diet-fed ADGAT DKO mice (Figure 3D). Glucose and insulin tolerances were similar in chow-diet-fed control and ADGAT DKO mice (Figures 3E and 3F). Thus, despite their lipodystrophy, ADGAT DKO mice had substantial levels of adipocyte-derived endocrine hormones and apparently normal glucose metabolism.

Lipodystrophy is also typically accompanied by ectopic lipid deposition, particularly manifesting as hepatic steatosis (Cui et al., 2011; Moitra et al., 1998; Shimomura et al., 1998). The livers of ADGAT DKO mice appeared normal (Figure 3G), with moderately increased weights in 15-week-old chow-diet-fed mice (1.7 ± 0.2 g vs. 2.1 ± 0.3 g, $p<0.05$). TG levels were only modestly increased (~10%) in livers of ADGAT DKO mice and were unchanged in skeletal muscle (Figure 3H). Thus, ADGAT DKO mice, with markedly reduced TG storage in adipose tissue, were remarkably metabolically healthy, with essentially none of the metabolic derangements typically associated with lipodystrophy.

ADGAT DKO mice are resistant to diet-induced obesity and associated metabolic derangements

We next tested whether the metabolically heathy phenotype of ADGAT DKO mice would persist with feeding of a western-type high-fat diet (HFD), which normally causes obesity and insulin resistance. We hypothesized that ADGAT DKO mice would ectopically accumulate fat, resulting in tissue lipotoxicity, because fatty acids from the HFD would not be stored in adipocytes. However, after feeding ADGAT DKO mice a HFD for 12 weeks, they appeared healthy and remained relatively lean, with both male and female mice gaining ~40% less body weight than control D1D2 flox mice (Figures 4A–4C). The reduction in body weight was due to a ~70% reduction in fat mass (Figure 4C). Food intake during HFD feeding was similar (Figure 4D), implying ADGAT DKO mice have increased energy expenditure. This was validated by indirect calorimetry, where ADGAT DKO mice exhibited increased energy expenditure that was particularly prominent during night-time, when the mice were eating (Figure 4E). The respiratory

exchange ratio (RER) was lower in ADGAT DKO mice during HFD feeding (Figure 4F), consistent with increased fat oxidation.

We also examined metabolic parameters in the HFD-fed ADGAT DKO mice. Plasma glucose levels were slightly lower in ADGAT DKO, and insulin levels were not different (Figures S4B and S4C). ADGAT DKO mice were protected from HFD-induced glucose intolerance and showed an enhanced insulin response (Figures 4G and 4H). Liver weights and hepatic TG levels were markedly increased with HFD in both ADGAT DKO mice and controls and were ~20% and ~10% higher in ADGAT DKO mice, respectively (Figure 4I). Hepatic cholesterol levels were similar (Figure 4I). HFD-induced activation of ER-stress response in the livers was similar to control mice (Figure S4D). Thus, surprisingly, despite not being able to robustly store TGs in adipocytes, ADGAT DKO mice were resistant to most effects of an HFD, and our studies indicate that they activate compensatory mechanisms of energy expenditure that increase fat oxidation.

ADGAT DKO mice activate energy dissipation mechanisms, including adipocyte beiging in WAT

We next investigated the mechanisms for improved metabolic health in ADGAT DKO mice. Browning or beiging of adipose tissue is associated with improved metabolic health in mice and humans (Becher et al., 2021; Kazak et al., 2015; van Marken Lichtenbelt et al., 2009; Wu et al., 2012), and the “beige” appearance in iWAT and gWAT depots of ADGAT DKO mice (Figures 1D and 1E) suggested that beiging adaptations may be present. Histological examination showed almost all adipocytes in both iWAT and gWAT contained multi-locular LDs (Figures 5A and 5C). mRNA levels of signature genes of adipocyte beiging, such as *Ucp1* (~600-fold), *CideA* (~20-fold), *Pparα* (~10-fold), and *Pgc1α* (~sixfold), were markedly increased in iWAT and gWAT of room temperature housed chow-fed ADGAT DKO mice (Figures 5B and 5D). Fatty acid levels were decreased; intermediates of glycolysis and Krebs cycle were enriched in both iWAT and BAT of ADGAT DKO mice, consistent with increased glycolysis and fatty acid oxidation (Figures S5A and S5B). Protein levels of UCP1 and respiratory complex proteins were also markedly greater in iWAT of room-temperature-housed chow-fed ADGAT DKO mice than controls and were even further increased under HFD conditions (Figure 5E). Beiging of adipocytes in iWAT appeared independent of ambient temperature and was also present in ADGAT DKO mice after 6 weeks of thermoneutral housing (Figure 5F), and blood glucose levels were moderately lower in thermoneutral housed male and female mice (Figure 5G). Beiging appeared to be non-cell-autonomous, as the changes found in beige fat were largely absent in differentiated pre-adipocytes, with the exception of a twofold increase of *Ucp1* mRNA levels (Figures S6A–S6D). Beiging is classically activated by the sympathetic nervous system (SNS) (Harms and Seale, 2013; Kajimura et al., 2015), and indeed, we found that markers of beiging were reduced with denervation of a fat pad (Figures S6E–S6G), indicating some contribution of the SNS to the beiging phenotype. Hormones, such as FGF21, also activate beiging, either

via the SNS (Fisher et al., 2012; Owen et al., 2014) or in a paracrine manner (Abu-Odeh et al., 2021; Fisher et al., 2012). In agreement with this possibility, FGF21 mRNA levels were increased by ~twofold and ~sixfold in liver and iWAT of ADGAT DKO mice, respectively (Figure S7A), and plasma levels of FGF21 were increased ~threefold in ADGAT KO mice (Figure S7B). However, plasma FGF21 levels were similar in ADGAT DKO mice and controls that were fed an HFD, suggesting an endocrine FGF21 effect is not responsible for the increased beiging of iWAT (Figures S7B–S7D).

DISCUSSION

We show here that the endocrine function of WAT can be uncoupled from fat storage. Remarkably, the resulting lipodystrophic ADGAT DKO mice with marked reductions in fat storage are metabolically healthy and do not develop metabolic derangements, such as diabetes or hepatic steatosis, even when fed an HFD. The metabolic health of the ADGAT DKO mice likely is due to their ability to maintain adequate adipose tissue endocrine function. Adipose tissue of ADGAT DKO mice maintained the ability to synthesize and secrete adipose-derived hormones, such as leptin, which is crucially absent in typical lipodystrophy (Garg, 2004; Savage, 2009). These findings are consistent with studies showing the importance of leptin in reversing many of the effects of lipodystrophy (Oral et al., 2002; Shimomura et al., 1999) and with studies emphasizing leptin's ability to prevent ectopic lipid accumulation and diabetes (Shimomura et al., 1999; Wang et al., 2010). Leptin levels often correlate with adiposity and TG stores (Maffei et al., 1995). The ADGAT DKO mouse model exhibits a dissociation of TG stores with leptin expression, thereby showing that these parameters appear not to be causally related. Instead, leptin levels may be better correlated with other adipose properties, such as the number of adipocytes.

Our studies revealed that, in response to the compromised ability to store TG in adipose tissue, mice activate pathways of energy expenditure, presumably including those in beige adipocytes and BAT. The mechanisms underlying the activation of energy expenditure and beiging in ADGAT-DKO mice are not clear at present, but appeared to involve control of the SNS, as fat-pad denervation partially reduced markers of beiging. Hormones that activate beiging, such as FGF21, are also testable candidate factors that may contribute to the ADGAT DKO phenotype. Many of the beneficial metabolic effects that we found in ADGAT DKO mice, including increased energy expenditure, increased glucose uptake by BAT, and torpor and browning, are found in murine models with increased levels of FGF21 (Fisher et al., 2012; Inagaki et al., 2007; Kwon et al., 2015; Owen et al., 2014). However, an endocrine effect of FGF21 seems unlikely in these mice due to similar levels of the hormone in plasma of HFD-fed mice. One possible mechanism for the beiging and increased energy expenditure is that the ADGAT DKO mice secrete (a) factor(s) that activates the SNS and beiging pathway. Although currently such a factor remains to be identified, this model is reminiscent of global DGAT1 knockout mice (Smith et al., 2000), which exhibit increased energy expenditure, enhanced glucose metabolism, protection from diet-induced obesity, and

increased leptin sensitivity (Chen et al., 2003; Chen et al., 2004; Chen et al., 2002). For global DGAT1 knockout mice, fat transplant studies suggested the adipose tissue is the source of such factors (Chen et al., 2003).

Our findings are consistent with our previous data showing that adipocytes differentiate normally in the absence of TG storage (Harris et al., 2011). Similarly, in this study, it appears that adipose tissue differentiates normally in the absence of TG storage. This is in contrast to the loss of function for AGPAT2, an enzyme that catalyzes an earlier step in the glycerolipid pathway, which results in impaired adipocyte differentiation. Also, deficiency of another glycerolipid synthesis enzyme, lipin 1, causes lipoatrophy in mice (Agarwal et al., 2002; Peterfy et al., 2001). Taken together, these findings suggest that an intermediate of glycerolipid synthesis, which is abnormal in AGPAT2 or lipin 1 deficiency but normal in DGAT1/2 deficiency, is required to promote normal adipocyte differentiation.

In summary, our studies provide new insights into the relationship between TG storage and endocrine function of adipose tissue. Murine adipose tissue with markedly depleted TG stores largely maintained its endocrine function and did not result in ectopic lipid accumulation and lipotoxicity. Instead, it led to activation of energy dissipation pathways, including beiging of WAT. Importantly, our findings show that lipodystrophy can be uncoupled from its metabolic consequences, and TG storage in WAT can be uncoupled from leptin production.

ACKNOWLEDGMENTS

We thank members of the Farese & Walther laboratory for helpful comments and G. Howard for editorial assistance. We thank Karen Inouye and Sarah Mitchell for helping with indirect calorimetry analysis. Nathan Heinzman for helping with metabolomics experiment and the Longwood small animal imaging facility at Beth Israel Deaconess Medical Center for PET/CT analysis. This work was supported in part by NIH grant R01GM124348 (to R.F.). T.C.W is an investigator of the Howard Hughes Medical Institute.

CONTRIBUTIONS

C.C., R.V.F., and T.C.W. planned the study and designed the experiments. C.C. generated DGAT2 flox, DGAT double flox and ADGAT DKO mice. C.C. performed most of the experiments. A.W.F. performed denervation of mice. K.W. analyzed metabolomics data. Y.A. performed lipidomics analysis. B.Y. and S.H. performed metabolomics. C.C., R.V.F., and T.C.W. wrote the manuscript. All authors read and edited the manuscript.

DECLARATION OF INTERESTS

T.C.W. is a consultant for Third Rock Ventures, and a founder and chairman of the scientific advisory board of Antora Bio. R.V.F. has consulted gratis for Third Rock Ventures on lipodystrophy.

STAR★METHODS

- KEY RESOURSES TABLE
- CONTACT FOR REAGENT AND RESOURSE SHARING
- EXPERIMENTAL MODEL AND SUBJECT DETAILS
  - Generation of ADGAT DKO mice
  - Animal Husbandry
  - Cold exposure Studies
- METHOD DETAILS
  - DGAT Activity Assay
  - Tissue Lipid Analysis
  - Microscopy and Image Processing
  - [^{18}F]-FDG-PET/CT Analysis
  - RNA extraction and Quantitative Real-Time PCR
  - Immunoblotting
  - Comprehensive Lab Animal Monitoring System (CLAMS)
  - Denervation of Adipose Tissue
- QUANTIFICAION AND STATISTICAL ANALYSIS

CONTACT FOR REAGENT AND RESOURCES SHARING

Further information and request for reagents and resources should be mailed to Robert V. Farese, Jr. (robert@hsph.harvard.edu) and Tobias C. Walther (twalther@hsph.harvard.edu).

KEY RESOURCES TABLE

REAGENT or RESOURCE	SOURCE	IDENTIFIER
Mice		
ADGAT DKO mice	This paper	N/A
Dgat1$^{flox/flox}$ mice	(Shih et al., 2009); The Jackson Laboratory	Cat # 017322
Dgat2$^{flox/flox}$ mice	(Chitraju et al., 2019); The Jackson Laboratory	Cat # 033518
Adipoq-Cre (Adiponectin-Cre) mice	(Eguchi et al., 2011); The Jackson Laboratory	Cat # 028020
Mouse Diets		
Chow-diet	PicoLab® Rodent Diet 20	Cat # 5053
Breeder's-diet	PicoLab® Rodent Diet 20	Cat # 5058
High-fat-diet	Envigo	Cat # TD.88137
Antibodies		
Rabbit polyclonal anti-DGAT1	In house (Chitraju et al., 2019)	N/A
Rabbit polyclonal anti-DGAT2	In house (Chitraju et al., 2019)	N/A
Rabbit polyclonal anti-UCP1	Abcam	Cat# ab10983
Total OXPHOS Rodent WB Antibody Cocktail	Abcam	Cat# ab110413
Rabbit monoclonal anti-GAPDH	Cell Signaling Technology	Cat# 5174S
Mouse monoclonal anti-α-Tubulin	Sigma-Aldrich	Cat# T9026
Chemicals, Peptides and Recombinant Proteins		
1,2-Dioleoyl-rac-glycerol	Sigma-Aldrich	Cat# D8394
Oleoyl coenzyme A lithium salt	Sigma-Aldrich	Cat# O1012
Oleoyl [14C] Coenzyme A	American Radiolabeled Chemicals, Inc.	Cat# ARC 0527
Oleic acid [14C]	American Radiolabeled Chemicals, Inc.	Cat# ARC 0297
Thin Layer Chromatography Plates	Analtech	Cat# P43911
Insulin	Lilly Corporation	Humulin R (U 100)
CL 316,243 hydrate	Sigma-Aldrich	Cat# C5976
Glycogen from bovine liver	Sigma-Aldrich	Cat# G0885
Protease inhibitors	Roche	Cat# 11873580001
Critical Commercial Assays		
Power SYBR Green PCR Master Mix	Life Technologies	Cat # 4368706
iScript™ cDNA Synthesis Kit	Biorad	Cat # 170-8891
RNeasy Mini Kit	Qiagen	Cat # 74106
QIAzol Lysis Reagent	Qiagen	Cat # 79306
QIAshredder	Qiagen	Cat# 79656
RNase-Free DNase Set	Qiagen	Cat# 79254
SuperSignal West Pico	ThermoFisher Scientific	Cat# 34580
SuperSignal West Femto	ThermoFisher Scientific	Cat# 34095
Infinity Triglycerides Reagent	Thermo Fisher	Cat # TR22421
Infinity Cholesterol Reagent	Thermo Fisher	Cat # TR13421
Free Glycerol Reagent	Sigma-Aldrich	Cat # F6428
HR Series NEFA-HR(2) Color Reagent A	FUJIFILM Medical Systems	Cat # 999-34691
HR Series NEFA-HR(2) Solvent A	FUJIFILM Medical Systems	Cat # 995-34791
HR Series NEFA-HR(2) Color Reagent B	FUJIFILM Medical Systems	Cat # 991-34891
HR Series NEFA-HR(2) Solvent B	FUJIFILM Medical Systems	Cat # 993-35191

EXPERIMENTAL PROCEDURES

Generation of ADGAT DKO Mice

To generate adipose tissue–specific *Dgat1* and *Dgat2* double-knockout (ADGAT DKO) mice, we first generated *Dgat1* and *Dgat2* double-floxed mice (D1D2 flox) by crossing *Dgat1*$^{flox/flox}$ mice (Shih et al., 2009) (Jackson Laboratory stock number: 017322) with *Dgat2*$^{flox/flox}$ mice (Chitraju et al., 2019) (Jackson Laboratory stock number: 033518). To generate ADGAT DKO mice, we crossed D1D2 flox mice with transgenic mice expressing Cre recombinase under control of the murine adiponectin promoter (Eguchi et al., 2011) (Jackson Laboratory stock number: 028020).

Animal Husbandry

All mouse experiments were performed under the guidelines from Harvard Center for Comparative Medicine. Mice were maintained in a barrier facility, at room temperatures (22–23ºC), on a regular 12-h light and 12-h dark cycle and had *ad libitum* access to food and water unless otherwise stated. For thermoneutral studies, mice were housed at 29ºC. Mice were fed on standard laboratory chow diet (PicoLab® Rodent Diet 20, 5053; less than 4.5% crude fat) or Western-type high-fat diet (Envigo, TD.88137; 21.2% fat by weight, 42% kcal from fat).

Cold-Exposure Studies

For cold-exposure experiments (at 5ºC), mice were single-housed in the morning around 8:00 am. Mice had free access to food and water unless otherwise stated. Core body temperatures were recorded using a rectal probe thermometer.

DGAT Activity Assay

DGAT enzymatic activity was measured in WAT and BAT lysates at V_{max} substrate concentrations. Assay mixture contained 20 µg of adipose tissue lysate, 100 µM of 1,2-dioleoyl-*sn*-glycerol, 25 µM of oleoyl-CoA, which contained [^{14}C] oleoyl-CoA as tracer, and 5 mM $MgCl_2$ in an assay in buffer containing 100 mM Tris-HCl (pH 7.4) and protease inhibitors. Reactions were carried out as described (Cases et al., 2001; Chitraju et al., 2017). After stopping the reaction, lipids were extracted and separated by TLC using a hexane:diethyl ether:acetic acid (80:20:1) solvent system. The TLC plates were exposed to phosphor imager screen and developed.

Tissue Lipid Analysis

Approximately 50 mg of adipose tissue was homogenized in 1 mL of lysis buffer (250 mM sucrose, 50 mM Tris Cl, pH 7.0, with protease inhibitor cocktail (11873580001, Roche)). The homogenate was mixed with 5 ml of chloroform: methanol (3:2 v:v) and extracted for 2 h by vigorous shaking. Upon centrifugation at 3000 x g at room temperature for 10 min, 100 µL of lower organic phase was collected and dried in a

speed vac. To the dried lipids, 100–300 µL of 0.1% Triton X-100 was added, and the solution was sonicated using ultrasonic homogenizer (Biologics, Inc., model 3000MP) for 10 sec with 30% amplitude. The total TG content was measured using the Infinity TM triglycerides reagent (Thermo Scientific) according to the manufacturer's protocol. TG and total cholesterol were measured using Infinity TM triglycerides reagent (Thermo Scientific) and a cholesterol E kit (Wako Diagnostics), respectively, according to manufacturer's protocol. For plasma lipids measurement, 5 µL of plasma was used directly.

Microscopy and Image Processing

Microscopy was performed on spinning disk confocal microscope (Yokogawa CSU-X1) set up on a Nikon Eclipse Ti inverted microscope with a 100× ApoTIRF 1.4 NA objective (Nikon) in line with 2x amplification. BODIPY 493/503 fluorophore was exited on 561-nm laser line. Fluorescence was detected by an iXon Ultra 897 EMCCD camera (Andor). Acquired images were processed using FIJI software (http://fiji.sc/Fiji).

RNA Extraction and Quantitative Real-Time PCR (qRT-PCR)

Total RNA from tissues was isolated with the Qiazol lysis reagent and using the protocol of the RNeasy Kit (Qiagen). Complementary DNA was synthesized using the iScript cDNA Synthesis Kit (Bio-Rad), and qPCRs were performed using the SYBR Green PCR Master Mix Kit (Applied Biosystems).

Immunoblotting

Tissues were lysed using RIPA lysis buffer (25 mM Tris Cl, pH 7.6, 150 mM NaCl, 1% NP-40, 1% sodium deoxycholate, 0.1% SDS) containing protease inhibitors (11873580001, Roche). Proteins were denatured in Laemmli buffer and separated on 10% SDS-PAGE gels and transferred to PVDF membranes (Bio-Rad). The membranes were blocked with blocking buffer for 1 h in TBST containing 5% BSA or 5% milk, and then incubated with primary antibodies overnight. The membranes were then washed three times with TBST for 10 min, and incubated in mouse secondary antibodies (Santa Cruz Biotechnology) at 1:5000 dilutions in blocking buffer. Membranes was washed again three times with TBST for 10 min, and revealed using the Super Signal West Pico kit (Thermo Scientific).

Comprehensive Lab Animal Monitoring System (CLAMS)

Mice were housed individually and acclimatized for 2 days. Oxygen consumption, carbon dioxide release, energy expenditure, and activity were measured using a Columbus Instruments' Oxymax Comprehensive Lab Animal Monitoring System (CLAMS) system according to guidelines for measuring energy metabolism in mice (Tschop et al., 2011).

Lipidomics Analysis

For lipidomic analysis of iWAT, ~50 mg of iWAT was homogenized in 1 mL ice-cold phosphate-buffered saline using a bead mill homogenizer. Tissue lysates (50 µg) were transferred to a pyrex glass tubes with a PTFE-liner cap. Lipids were extracted by Folch method (Folch et al., 1957), briefly, 6 mL of ice-cold chloroform-methanol (2:1 v/v) and 1.5 mL of water were added to the samples, and tubes were vortexed thoroughly to mix the samples homogenously with a polar and non-polar solvent. SPLAH mix internal standards were spiked in before the extraction. The organic phase of each sample was normalized by total soluble protein amounts and measured by BCA assay (Thermo Scientific, 23225, Waltham, MA). After vortexing, samples were centrifuged for 30 min at 1100 rpm at 4ºC to separate the organic and inorganic phases. Using a sterile glass pipette, the lower organic phase was transferred into a new glass tube, taking care to avoid the intermediate layer of cellular debris and precipitated proteins. The samples were dried under nitrogen flow until the solvents were completely dried. Samples were resuspended in 250 µL of chloroform: methanol 2:1 and stored in -80 until mass spectrometer (MS) analysis. Lipids were separated using ultra-high-performance liquid chromatography (UHPLC) coupled with tandem MS. Briefly, UHPLC analysis was performed on a C30 reverse-phase column (Thermo Acclaim C30, 2.1 x 250 mm, 3 µm operated at 55° C; Thermo Fisher Scientific) connected to a Dionex UltiMate 3000 HPLC system and a QExactive orbitrap MS (Thermo Fisher Scientific) equipped with a heated electrospray ionization probe. 5 µL of each sample was analyzed separately, using positive and negative ionization modes. Mobile phase contained 60:40 water:acetonitrile (v:v), 10 mM ammonium formate and 0.1% formic acid, and mobile phase B consisted of 90:10 2-propanol/acetonitrile, also including 10 mM ammonium formate and 0.1% formic acid. MS spectra of lipids were acquired in full-scan/data-dependent MS2 mode. For the full-scan acquisition, the resolution was set to 70,000, the AGC target was 1e6, the maximum injection time was 50 msec, and the scan range was m/z = 133.4–2000. For data-dependent MS2, the top 10 ions in each full scan were isolated with a 1.0 Da window, fragmented at a stepped normalized collision energy of 15, 25, and 35 units, and analyzed at a resolution of 17,500 with an AGC target of 2e5 and a maximum injection time of 100 msec. Peak identification and data analysis were carried out using Lipid Search software version 4.1 SP (Thermo Fisher Scientific) (Taguchi and Ishikawa, 2010).

Metabolomic Analysis

BAT and iWAT was snap frozen in liquid nitrogen and ground at cryogenic temperature with a cyromill (Retsch, Newtown, PA). The tissue was extracted with -20˚C 40: 40: 20 methanol: acetonitrile: water at a concentration of 25 mg/mL. Samples were vigorously vortexed and centrifuged at 4 ˚C at 16,000 g for 10 min, and the supernatant was transferred to LC-MS vials for analysis. Chromatographic separation was performed using XBridge BEH Amide XP Column (2.5 µm, 2.1 mm × 150 mm) with associated guard

column (2.5 µm, 2.1 mm X 5 mm) (Waters, Milford, MA). The mobile phase A was 95% water and 5% acetonitrile, containing 10 mM ammonium hydroxide and 10 mM ammonium acetate. The mobile phase B was 80% acetonitrile and 20% water, with 10 mM ammonium hydroxide and 10 mM ammonium acetate. The linear elution gradient was: 0 ~ 3 min, 100% B; 3.2 ~ 6.2 min, 90% B; 6.5. ~ 10.5 min, 80% B; 10.7 ~ 13.5 min, 70% B; 13.7 ~ 16 min, 45% B; and 16.5 ~ 22 min, 100% B. The flow rate was 0.3 mL/ min. The autosampler was maintained at 4˚C. The injection volume was 5 µL, and needle wash was performed between samples using 40: 40: 20 methanol: acetonitrile: water. The MS used was Q Exactive HF (Thermo Fisher Scientific, San Jose, CA), and scanned from 70 to 1000 *m/z* with switching polarity. The resolution was 120,000. Metabolites were identified based on accurate mass and retention time using an in-house library, and the software used was EI-Maven (Elucidata, Cambridge, MA). Data was analyzed using R software (version 4.2.0). The ion intensity of each sample was first normalized to the corresponding sample protein content. Differentially abundant metabolites were analyzed with the limma R/Bioconductor package, and the multiple comparisons were corrected using the Benjamini-Hochberg procedure (adjusted *p* value; q value). The volcano plots were generated using the ggplot and ggrepel packages.

Chemical Denervation of iWAT

Survival surgeries in mice were performed under the guidelines from Harvard Center for Comparative Medicine. Chemical denervation of inguinal adipose tissue was performed as described (Vaughan et al., 2014) by intra-fat injection of the catecholaminergic neurotoxin, 6-hydroxy-dopamine (6-OHDA). For injections, a solution of 6-OHDA (9 mg/ml) was prepared in PBS containing 1% ascorbic acid. Mice were anesthetized and fur was shaved in the target area and wiped the area with 95% ethanol. A small incision (~5 mm) was made to open iWAT depots without damaging fat pad and vasculature. Using 10-µL Hamilton syringe, 2 µL injections of 6-OHDA (9 mg/ml) were injected in 12 locations along iWAT depot. Sterile sutures were used to close incisions. Analgesic was administered, and mice were monitored daily.

Statistical Analyses

Data are presented as mean ± SD (standard deviation). Statistical significance was evaluated by unpaired two-tailed Student's t-test or two-way ANOVA with Bonferroni's multiple comparison test. Significant differences are annotated as follows: *p < 0.05, **p < 0.01, ***p < 0.001.

REFERENCES

Abu-Odeh, M., Zhang, Y., Reilly, S.M., Ebadat, N., Keinan, O., Valentine, J.M., Hafezi-Bakhtiari, M., Ashayer, H., Mamoun, L., Zhou, X., et al. (2021). FGF21 promotes thermogenic gene expression as an autocrine factor in adipocytes. Cell Rep *35*, 109331.

Agarwal, A.K., Arioglu, E., De Almeida, S., Akkoc, N., Taylor, S.I., Bowcock, A.M., Barnes, R.I., and Garg, A. (2002). AGPAT2 is mutated in congenital generalized lipodystrophy linked to chromosome 9q34. Nat Genet *31*, 21-23.

Agostini, M., Schoenmakers, E., Mitchell, C., Szatmari, I., Savage, D., Smith, A., Rajanayagam, O., Semple, R., Luan, J., Bath, L., et al. (2006). Non-DNA binding, dominant-negative, human PPARgamma mutations cause lipodystrophic insulin resistance. Cell Metab *4*, 303-311.

Becher, T., Palanisamy, S., Kramer, D.J., Eljalby, M., Marx, S.J., Wibmer, A.G., Butler, S.D., Jiang, C.S., Vaughan, R., Schoder, H., et al. (2021). Brown adipose tissue is associated with cardiometabolic health. Nat Med *27*, 58-65.

Cases, S., Smith, S.J., Zheng, Y.W., Myers, H.M., Lear, S.R., Sande, E., Novak, S., Collins, C., Welch, C.B., Lusis, A.J., et al. (1998). Identification of a gene encoding an acyl CoA:diacylglycerol acyltransferase, a key enzyme in triacylglycerol synthesis. Proc Natl Acad Sci U S A *95*, 13018-13023.

Cases, S., Stone, S.J., Zhou, P., Yen, E., Tow, B., Lardizabal, K.D., Voelker, T., and Farese, R.V., Jr. (2001). Cloning of DGAT2, a second mammalian diacylglycerol acyltransferase, and related family members. J Biol Chem *276*, 38870-38876.

Chen, H.C., Jensen, D.R., Myers, H.M., Eckel, R.H., and Farese, R.V., Jr. (2003). Obesity resistance and enhanced glucose metabolism in mice transplanted with white adipose tissue lacking acyl CoA:diacylglycerol acyltransferase 1. J Clin Invest *111*, 1715-1722.

Chen, H.C., Rao, M., Sajan, M.P., Standaert, M., Kanoh, Y., Miura, A., Farese, R.V., Jr., and Farese, R.V. (2004). Role of adipocyte-derived factors in enhancing insulin signaling in skeletal muscle and white adipose tissue of mice lacking Acyl CoA:diacylglycerol acyltransferase 1. Diabetes *53*, 1445-1451.

Chen, H.C., Smith, S.J., Ladha, Z., Jensen, D.R., Ferreira, L.D., Pulawa, L.K., McGuire, J.G., Pitas, R.E., Eckel, R.H., and Farese, R.V., Jr. (2002). Increased insulin and leptin sensitivity in mice lacking acyl CoA:diacylglycerol acyltransferase 1. J Clin Invest *109*, 1049-1055.

Chitraju, C., Fischer, A.W., Farese, R.V., Jr., and Walther, T.C. (2020). Lipid Droplets in Brown Adipose Tissue Are Dispensable for Cold-Induced Thermogenesis. Cell Rep *33*, 108348.

Chitraju, C., Mejhert, N., Haas, J.T., Diaz-Ramirez, L.G., Grueter, C.A., Imbriglio, J.E., Pinto, S., Koliwad, S.K., Walther, T.C., and Farese, R.V., Jr. (2017). Triglyceride Synthesis by DGAT1 Protects Adipocytes from Lipid-Induced ER Stress during Lipolysis. Cell Metab *26*, 407-418 e403.

Chitraju, C., Walther, T.C., and Farese, R.V., Jr. (2019). The triglyceride synthesis enzymes DGAT1 and DGAT2 have distinct and overlapping functions in adipocytes. J Lipid Res *60*, 1112-1120.

Cui, X., Wang, Y., Tang, Y., Liu, Y., Zhao, L., Deng, J., Xu, G., Peng, X., Ju, S., Liu, G., et al. (2011). Seipin ablation in mice results in severe generalized lipodystrophy. Hum Mol Genet *20*, 3022-3030.

Eguchi, J., Wang, X., Yu, S., Kershaw, E.E., Chiu, P.C., Dushay, J., Estall, J.L., Klein, U., Maratos-Flier, E., and Rosen, E.D. (2011). Transcriptional control of adipose lipid handling by IRF4. Cell Metab *13*, 249-259.

Fisher, F.M., Kleiner, S., Douris, N., Fox, E.C., Mepani, R.J., Verdeguer, F., Wu, J., Kharitonenkov, A., Flier, J.S., Maratos-Flier, E., et al. (2012). FGF21 regulates PGC-1alpha and browning of white adipose tissues in adaptive thermogenesis. Genes Dev *26*, 271-281.

Folch, J., Lees, M., and Sloane Stanley, G.H. (1957). A simple method for the isolation and purification of total lipides from animal tissues. J Biol Chem *226*, 497-509.

Friedman, J.M. (2019). Leptin and the endocrine control of energy balance. Nat Metab *1*, 754-764.

Gandotra, S., Le Dour, C., Bottomley, W., Cervera, P., Giral, P., Reznik, Y., Charpentier, G., Auclair, M., Delepine, M., Barroso, I., et al. (2011). Perilipin deficiency and autosomal dominant partial lipodystrophy. N Engl J Med *364*, 740-748.

Garg, A. (2004). Acquired and inherited lipodystrophies. N Engl J Med *350*, 1220-1234.

Harms, M., and Seale, P. (2013). Brown and beige fat: development, function and therapeutic potential. Nat Med *19*, 1252-1263.

Harris, C.A., Haas, J.T., Streeper, R.S., Stone, S.J., Kumari, M., Yang, K., Han, X., Brownell, N., Gross, R.W., Zechner, R., et al. (2011). DGAT enzymes are required for triacylglycerol synthesis and lipid droplets in adipocytes. J Lipid Res *52*, 657-667.

Hegele, R.A., Cao, H., Frankowski, C., Mathews, S.T., and Leff, T. (2002). PPARG F388L, a transactivation-deficient mutant, in familial partial lipodystrophy. Diabetes *51*, 3586-3590.

Inagaki, T., Dutchak, P., Zhao, G., Ding, X., Gautron, L., Parameswara, V., Li, Y., Goetz, R., Mohammadi, M., Esser, V., et al. (2007). Endocrine regulation of the fasting response by PPARalpha-mediated induction of fibroblast growth factor 21. Cell Metab *5*, 415-425.

Kajimura, S., Spiegelman, B.M., and Seale, P. (2015). Brown and Beige Fat: Physiological Roles beyond Heat Generation. Cell Metab *22*, 546-559.

Kazak, L., Chouchani, E.T., Jedrychowski, M.P., Erickson, B.K., Shinoda, K., Cohen, P., Vetrivelan, R., Lu, G.Z., Laznik-Bogoslavski, D., Hasenfuss, S.C., et al. (2015). A creatine-driven substrate cycle enhances energy expenditure and thermogenesis in beige fat. Cell *163*, 643-655.

Kershaw, E.E., and Flier, J.S. (2004). Adipose tissue as an endocrine organ. J Clin Endocrinol Metab *89*, 2548-2556.

Kwon, M.M., O'Dwyer, S.M., Baker, R.K., Covey, S.D., and Kieffer, T.J. (2015). FGF21-Mediated Improvements in Glucose Clearance Require Uncoupling Protein 1. Cell Rep *13*, 1521-1527.

Lawrence, R.D. (1946). Lipodystrophy and hepatomegaly with diabetes, lipaemia, and other metabolic disturbances; a case throwing new light on the action of insulin. (concluded). Lancet *1*, 773.

Lim, K., Haider, A., Adams, C., Sleigh, A., and Savage, D.B. (2021). Lipodistrophy: a paradigm for understanding the consequences of "overloading" adipose tissue. Physiol Rev *101*, 907-993.

Maffei, M., Halaas, J., Ravussin, E., Pratley, R.E., Lee, G.H., Zhang, Y., Fei, H., Kim, S., Lallone, R., Ranganathan, S., et al. (1995). Leptin levels in human and rodent: measurement of plasma leptin and ob RNA in obese and weight-reduced subjects. Nat Med *1*, 1155-1161.

Magre, J., Delepine, M., Khallouf, E., Gedde-Dahl, T., Jr., Van Maldergem, L., Sobel, E., Papp, J., Meier, M., Megarbane, A., Bachy, A., et al. (2001). Identification of the gene altered in Berardinelli-Seip congenital lipodystrophy on chromosome 11q13. Nat Genet *28*, 365-370.

Mann, J.P., and Savage, D.B. (2019). What lipodystrophies teach us about the metabolic syndrome. J Clin Invest *129*, 4009-4021.

Misra, A., and Garg, A. (2003). Clinical features and metabolic derangements in acquired generalized lipodystrophy: case reports and review of the literature. Medicine (Baltimore) *82*, 129-146.

Moitra, J., Mason, M.M., Olive, M., Krylov, D., Gavrilova, O., Marcus-Samuels, B., Feigenbaum, L., Lee, E., Aoyama, T., Eckhaus, M., et al. (1998). Life without white fat: a transgenic mouse. Genes Dev *12*, 3168-3181.

Oral, E.A., Simha, V., Ruiz, E., Andewelt, A., Premkumar, A., Snell, P., Wagner, A.J., DePaoli, A.M., Reitman, M.L., Taylor, S.I., et al. (2002). Leptin-replacement therapy for lipodystrophy. N Engl J Med *346*, 570-578.

Owen, B.M., Ding, X., Morgan, D.A., Coate, K.C., Bookout, A.L., Rahmouni, K., Kliewer, S.A., and Mangelsdorf, D.J. (2014). FGF21 acts centrally to induce sympathetic nerve activity, energy expenditure, and weight loss. Cell Metab *20*, 670-677.

Patni, N., and Garg, A. (2015). Congenital generalized lipodystrophies--new insights into metabolic dysfunction. Nat Rev Endocrinol *11*, 522-534.

Peterfy, M., Phan, J., Xu, P., and Reue, K. (2001). Lipodystrophy in the fld mouse results from mutation of a new gene encoding a nuclear protein, lipin. Nat Genet *27*, 121-124.

Reitman, M.L. (2002). Metabolic lessons from genetically lean mice. Annu Rev Nutr *22*, 459-482.

Reue, K., and Phan, J. (2006). Metabolic consequences of lipodystrophy in mouse models. Curr Opin Clin Nutr Metab Care *9*, 436-441.

Savage, D.B. (2009). Mouse models of inherited lipodystrophy. Dis Model Mech *2*, 554-562.

Scheja, L., and Heeren, J. (2019). The endocrine function of adipose tissues in health and cardiometabolic disease. Nat Rev Endocrinol *15*, 507-524.

Shih, M.Y., Kane, M.A., Zhou, P., Yen, C.L., Streeper, R.S., Napoli, J.L., and Farese, R.V., Jr. (2009). Retinol Esterification by DGAT1 Is Essential for Retinoid Homeostasis in Murine Skin. J Biol Chem *284*, 4292-4299.

Shimomura, I., Hammer, R.E., Ikemoto, S., Brown, M.S., and Goldstein, J.L. (1999). Leptin reverses insulin resistance and diabetes mellitus in mice with congenital lipodystrophy. Nature *401*, 73-76.

Shimomura, I., Hammer, R.E., Richardson, J.A., Ikemoto, S., Bashmakov, Y., Goldstein, J.L., and Brown, M.S. (1998). Insulin resistance and diabetes mellitus in transgenic mice expressing nuclear SREBP-1c in adipose tissue: model for congenital generalized lipodystrophy. Genes Dev *12*, 3182-3194.

Smith, S.J., Cases, S., Jensen, D.R., Chen, H.C., Sande, E., Tow, B., Sanan, D.A., Raber, J., Eckel, R.H., and Farese, R.V., Jr. (2000). Obesity resistance and multiple mechanisms of triglyceride synthesis in mice lacking Dgat. Nat Genet *25*, 87-90.

Stone, S.J., Myers, H.M., Watkins, S.M., Brown, B.E., Feingold, K.R., Elias, P.M., and Farese, R.V., Jr. (2004). Lipopenia and skin barrier abnormalities in DGAT2-deficient mice. J Biol Chem *279*, 11767-11776.

Taguchi, R., and Ishikawa, M. (2010). Precise and global identification of phospholipid molecular species by an Orbitrap mass spectrometer and automated search engine Lipid Search. J Chromatogr A *1217*, 4229-4239.

Tschop, M.H., Speakman, J.R., Arch, J.R., Auwerx, J., Bruning, J.C., Chan, L., Eckel, R.H., Farese, R.V., Jr., Galgani, J.E., Hambly, C., et al. (2011). A guide to analysis of mouse energy metabolism. Nat Methods *9*, 57-63.

van Marken Lichtenbelt, W.D., Vanhommerig, J.W., Smulders, N.M., Drossaerts, J.M., Kemerink, G.J., Bouvy, N.D., Schrauwen, P., and Teule, G.J. (2009). Cold-activated brown adipose tissue in healthy men. N Engl J Med *360*, 1500-1508.

Vaughan, C.H., Zarebidaki, E., Ehlen, J.C., and Bartness, T.J. (2014). Analysis and measurement of the sympathetic and sensory innervation of white and brown adipose tissue. Methods Enzymol *537*, 199-225.

Wang, M.Y., Chen, L., Clark, G.O., Lee, Y., Stevens, R.D., Ilkayeva, O.R., Wenner, B.R., Bain, J.R., Charron, M.J., Newgard, C.B., et al. (2010). Leptin therapy in insulin-deficient type I diabetes. Proc Natl Acad Sci U S A *107*, 4813-4819.

Wu, J., Bostrom, P., Sparks, L.M., Ye, L., Choi, J.H., Giang, A.H., Khandekar, M., Virtanen, K.A., Nuutila, P., Schaart, G., et al. (2012). Beige adipocytes are a distinct type of thermogenic fat cell in mouse and human. Cell *150*, 366-376.

Yen, C.L., Brown, C.H.t., Monetti, M., and Farese, R.V., Jr. (2005). A human skin multifunctional O-acyltransferase that catalyzes the synthesis of acylglycerols, waxes, and retinyl esters. J Lipid Res *46*, 2388-2397.

Zhang, Y., Proenca, R., Maffei, M., Barone, M., Leopold, L., and Friedman, J.M. (1994). Positional cloning of the mouse obese gene and its human homologue. Nature *372*, 425-432.

FIGURE LEGENDS

Figure 1. ADGAT DKO mice have reduced fat mass and triglycerides in adipose tissue.

(A) Chow-diet-fed ADGAT DKO mice appear normal. Representative photographs of control and ADGAT DKO mice fed a chow diet.

(B) Fat depots were decreased in ADGAT DKO mice. Nuclear magnetic resonance imaging of chow-diet-fed mice.

(C) ADGAT DKO mice have decreased fat mass. Dual-energy X-ray absorptiometry (DEXA) analysis of lean mass and fat mass of chow-diet-fed mice (n=8).

(D) Fat depots were atrophied in ADGAT DKO mice. Representative photographs of iWAT and gWAT (n=8).

(E) gWAT and iWAT of ADGAT DKO mice contain multilocular lipid droplets in adipocytes. H&E-stained sections of gWAT and iWAT from chow-diet-fed mice (n=6). Scale bars, 50 μm.

(F) WAT and BAT of ADGAT DKO mice were denser than controls and sink in an aqueous buffer with fixative (1.25% formaldehyde, 2.5% glutaraldehyde and 0.03% picric acid in 0.1 M sodium cacodylate buffer, pH 7.4, density = 1.01 g/mL) used to fix for electron microscopy.

(G) LDs in iWAT of ADGAT DKO mice are BODIPY positive. Confocal fluorescence microscopy images of adipose tissue. LDs were stained by BODIPY 493/503. Scale bar, 25 μm.

(H) WAT of ADGAT DKO mice contain triglycerides. Thin layer chromatography analysis of lipids from iWAT (n=4). TG, triglycerides; CE, cholesterol esters, FFA, free fatty acids; DAG, diacylglycerol.

(I) Increased phospholipid levels in iWAT of ADGAT DKO mice. Lipids in iWAT were extracted and quantified by mass spectrometry (n=8).

Data are presented as mean ± SD. *p<0.05, ***p<0.001.

Figure 2. Adipose tissue TG stores are required to prevent a torpor-like state during fasting.

(A) Body weights of mice fed *ad libitum* or fasted 14 h (n=10). Ad lib., *ad libitum* fed.

(B) Core body temperature of mice housed at room temperature and fed *ad libitum* or fasted for 14 h (n=10).

(C) Blood glucose levels in mice fed *ad libitum* or fasted for 14 h (n=8).

(D) Levels of plasma ketone bodies in mice fed *ad libitum* or fasted for 14 h (n=8).

(E and F) Core body temperature of mice housed in cold (5º Celsius) with or without food (n=10).

Data are presented as mean ± SD. *p<0.05, **p<0.01, ***p<0.001.

Figure 3. Lipodystrophy is uncoupled from detrimental metabolic effects in ADGAT DKO mice.

(A) Adiponectin and leptin mRNA levels were moderately increased in iWAT of ADGAT DKO mice. Relative mRNA levels of leptin and adiponectin in iWAT of chow-diet-fed mice (n=6).

(B) Plasma levels of adiponectin were normal, and leptin levels were moderately decreased in *ad libitum* chow-diet-fed mice (n=8).

(C) ADGAT DKO mice had normal glucose and insulin levels. Glucose and insulin levels in *ad libitum* chow-diet-fed mice (n=8).

(D) Decreased free fatty acids and ketones in ADGAT DKO mice. Levels of plasma metabolites in *ad libitum* chow-diet-fed mice (n=8).

(E and F) Glucose- and insulin-tolerance tests were normal in chow-diet-fed mice (n=10).

(G) ADGAT DKO mice had non-steatotic livers. Representative photographs of livers from chow-diet-fed mice.

(H) Triglyceride were moderately increased in livers of ADGAT DKO mice. Triglyceride levels in livers and skeletal muscle of chow-diet-fed mice (n=6).

Data are presented as mean ± SD. *p<0.05, **p<0.01, ***p<0.001.

Figure 4. ADGAT DKO mice are resistant to diet-induced obesity and glucose intolerance.

(A) ADGAT DKO mice stay lean on an HFD. Representative photographs of mice fed on HFD for 12 weeks.

(B) Both male and female ADGAT DKO mice gained ~40% less body weight than control mice. Body weights of mice fed on a chow-diet or HFD (n=15 for males, n=12 for females).

(C) ADGAT DKO mice had decreased fat mass on HFD feeding. DEXA analysis of lean mass and fat mass of HFD fed mice (n=10).

(D) ADGAT DKO mice had normal food intake during HFD feeding (n=5).

(E and F) ADGAT DKO mice had increased energy expenditures. Energy expenditure and respiratory quotient on HFD-fed mice measured by indirect calorimetry. Values were normalized to lean mass (n=4).

(G and H) ADGAT DKO mice were protected from HFD-induced glucose intolerance and insulin resistance. Glucose- and insulin-tolerance tests were performed on HFD-fed (for 9 or 10 weeks, respectively) mice (n=10I)

(I) Liver weights and triglyceride levels were moderately increased in HFD-fed ADGAT DKO mice (n=6).

Data are presented as mean ± SD. *p<0.05, **p<0.01, ***p<0.001.

Figure 5. Beiging of WAT in ADGAT DKO mice.

(A) ADGAT DKO mice contain multi-locular LDs in adipocytes of iWAT. H&E-stained sections of iWAT from mice fed a chow diet and housed at room temperature (n=6). Scale bars, 50 μm.

(B) Increased expression of thermogenic marker genes in iWAT of ADGAT DKO mice. Relative mRNA levels of thermogenic genes in iWAT of mice fed a chow diet and housed at room temperature (n=6).

(C) ADGAT DKO mice contain multi-locular LDs in adipocytes of gWAT. H&E-stained sections of gWAT from mice fed a chow diet and housed at room temperature (n=6). Scale bars, 50 μm.

(D) Increased expression of thermogenic marker genes in gWAT of ADGAT DKO mice. Relative mRNA levels of thermogenic genes in gWAT of mice fed a chow diet and housed at room temperature (n=6).

(E) HFD feeding increases levels of UCP1 in iWAT of ADGAT DKO mice. Immunoblot analysis of UCP1 and OXPHOS proteins in iWAT mice fed either a chow diet or an HFD (n=3). Mice were housed at room temperature.

(F) Beiging was intact in iWAT of thermoneutral-housed ADGAT DKO mice. Relative mRNA levels of thermogenic genes in iWAT of chow-diet-fed mice housed at thermoneutral temperature for 6 weeks (n=6).

(G) Blood glucose levels were normal in thermoneutral housed ADGAT DKO mice. Glucose levels in mice fed a chow diet and housed at thermoneutral temperature for 6 weeks (n=8).

Data are presented as mean ± SD. *p<0.05, **p<0.01, ***p<0.001.

SUPPLEMENTAL INFORMATION

FIGURE LEGENDS FOR SUPPLEMENTAL FIGURES

Figure S1. Related to Figure 1.

(A) *Dgat1* and *Dgat2* transcripts levels were decreased in iWAT and BAT of ADGAT DKO mice. Relative mRNA levels in iWAT and BAT of mice fed a chow diet (n=6).

(B) DGAT1 and DGAT2 proteins were absent in iWAT and BAT of ADGAT DKO mice. Western blot analysis of DGAT1 and DGAT2 in iWAT and BAT of mice fed a chow diet (n=4).

(C) *In-vitro* DGAT activity was decreased in lysates of iWAT and BAT of ADGAT DKO mice (n=4).

(D) Body weights, lean mass and fat mass analysis of 1-year-old mice fed a chow diet (n=10).

(E) Gross appearance of WAT depots in mice. **p<0.01, ***p<0.001.

Figure S2. Related to Figure 1.

(A) Gross appearance of BAT.

(B) H&E-stained sections of iBAT (n=6). Scale bars, 50 μm.

(C) Triglycerides and total cholesterol levels in BAT (n=6).

(D) [^{18}F]-FDG-PET/CT scans of mice administered CL 316,243.

(E) Glycogen levels in iBAT (n=6).

Data are presented as mean ± SD. ***p<0.001.

Figure S3. Related to Figure 1.

(A) Triglycerides were decreased in iWAT of ADGAT DKO mice (n=6). Triglyceride levels were measured using Infinity triglyceride reagent.

(B) Diacylglycerol and mono alkyl-diacylglycerol were decreased in iWAT of ADGAT DKO mice (n=6). Lipids were quantified by mass spectrometry.

(C) Triglyceride molecular species were decreased in iWAT of ADGAT DKO mice (n=6). Lipids were quantified by mass spectrometry.

Data are presented as mean ± SD. *p<0.05, **p<0.01, ***p<0.001.

Figure S4. Related to Figure 4.

(A) LDs isolated from iWAT of mice fed an HFD.

(B) Blood glucose levels in high-fat-diet fed mice (n=8).

(C) Insulin levels in high-fat-diet fed mice (n=8).

(D) Relative mRNA levels in livers of HFD mice (n=6).

Data are presented as mean ± SD. *p<0.05, **p<0.01, ***p<0.001.

Figure S5. Related to Figure 5.

(A) Volcano plot showing differentially abundant metabolites in iWAT of chow-diet-fed mice (n=8).

(B) Volcano plot showing differentially abundant metabolites in iBAT of chow-diet-fed mice (n=8).

Orange dots represent metabolites with more than twofold change (adjusted p values or q<0.05)). Blue dots represent metabolites with more than twofold change but not statistically significant. Grey dots represent metabolites that were unchanged between control and ADGAT DKO mice.

Figure S6. Related to Figure 5.

(A) Primary adipocytes differentiated from stromal vascular fraction of iWAT from ADGAT DKO mice contain lipid droplets. LDs were stained by BODIPY 493/503.

(B and C) Western blot analysis of DGATs and UCP1 in primary adipocytes (n=3).

(D) Relative mRNA levels in day-8 primary adipocytes loaded with oleic acid for 16 h (n=3).

(E) Body weights of denervated (iWAT) mice fed on an HFD (n=6).

(F) Blood glucose levels in denervated mice fed an HFD (n=6).

(G) Relative mRNA levels in iWAT of denervated mice fed an HFD (n=6).

Data are presented as mean ± SD. *p<0.05, **p<0.01, ***p<0.001.

Figure S7. Related to Figure 5.

(A) FGF21 transcript levels were increased in iWAT and livers of ADGAT DKO mice. Relative mRNA levels of FGF21 in iWAT and livers of chow-diet fed mice (n=6).

(B) FGF21 levels were increased in ADGAT DKO mice. Plasma levels of FGF21 in chow-diet-fed (*ad libitum* fed or 14 h fasted) or HFD-fed mice (n=8).

(C) FGF21 transcript levels in livers of chow-diet- or HFD-fed mice (n=6).

(D) Triglyceride levels in livers of chow-diet- or HFD-fed mice (n=6).

Data are presented as mean ± SD. *p<0.05, **p<0.01, ***p<0.001.

Supplementary Table S1.

Primers used for quantitative real-time PCR analysis of mouse genes		
Dgat1	Fwd:	GGAATATCCCCGTGCACAA
	Rev:	CATTTGCTGCTGCCATGTC
Dgat2	Fwd:	CCGCAAAGGCTTTGTGAA
	Rev:	GGAATAAGTGGGAACCAGATCAG
Srebp1c	Fwd:	GGAGCCATGGATTGCACATT
	Rev:	GGCCCGGGAAGTCACTGT
Acc	Fwd:	GATGAACCATCTCCGTTGGC
	Rev:	GACCCAATTATGAATCGGGAGTG
Fas	Fwd:	GGAGGTGGTGATAGCCGGTAT
	Rev:	TGGGTAATCCATAGAGCCCAG
Scd1	Fwd:	TTCTTGCGATACACTCTGGTGC
	Rev:	CGGGATTGAATGTTCTTGTCGT
Ucp1	Fwd:	AGGCTTCCAGTACCATTAGGT
	Rev:	CTGAGTGAGGCAAAGCTGATTT
CideA	Fwd:	TGCTCTTCTGTATCGCCCAGT
	Rev:	GCCGTGTTAAGGAATCTGCTG
*Pgc1*α	Fwd:	TTCATCTGAGTATGGAGTCGCT
	Rev:	GGGGGTGAAACCACTTTTGTAA
*Ppar1*α	Fwd:	AATGCAATTCGCTTTGGAAG
	Rev:	GGCCTTGACCTTGTTCATGT
*Cpt1*α	Fwd:	GAACCCCAACATCCCCAAAC
	Rev:	TCCTGGCATTGTCCTGGAAT
Mcad	Fwd:	AGGTTTCAAGATCGCAATGG
	Rev:	CTCCTTGGTGCTCCACTAGC
Lcad	Fwd:	TCCATGGCAAAATACTGGGC
	Rev:	TTGCAATCGGGTACTCCCAC
Xbp1s	Fwd:	GGTCTGCTGAGTCCGCAGCAGG
	Rev:	AGGCTTGGTGTATACATGG
Chop	Fwd:	CCACCACACCTGAAAGCAGAA
	Rev:	AGGTGAAAGGCAGGGACTCA
Bip	Fwd:	ACTTGGGGACCACCTATTCCT
	Rev:	ATCGCCAATCAGACGCTCC
Atf3	Fwd:	GAGGATTTTGCTAACCTGACACC
	Rev:	TTGACGGTAACTGACTCCAGC
Atf4	Fwd:	CCTTCGACCAGTCGGGTTTG
	Rev:	CTGTCCCGGAAAAGGCATCC
Tnfα	Fwd:	CCCTCACACTCAGATCATCTTCT
	Rev:	GCTACGACGTGGGCTACAG
F4/80	Fwd:	TGACTCACCTTGTGGTCCTAA
	Rev:	CTTCCCAGAATCCAGTCTTTCC
Fgf21	Fwd:	GTGTCAAAGCCTCTAGGTTTCTT
	Rev:	GGTACACATTGTAACCGTCCTC
Cyclophilin	Fwd:	GGAGATGGCACAGGAGGAAA
	Rev:	CCGTAGTGCTTCAGTTTGAAGTTCT
Fwd, forward; Rev, reverse.		

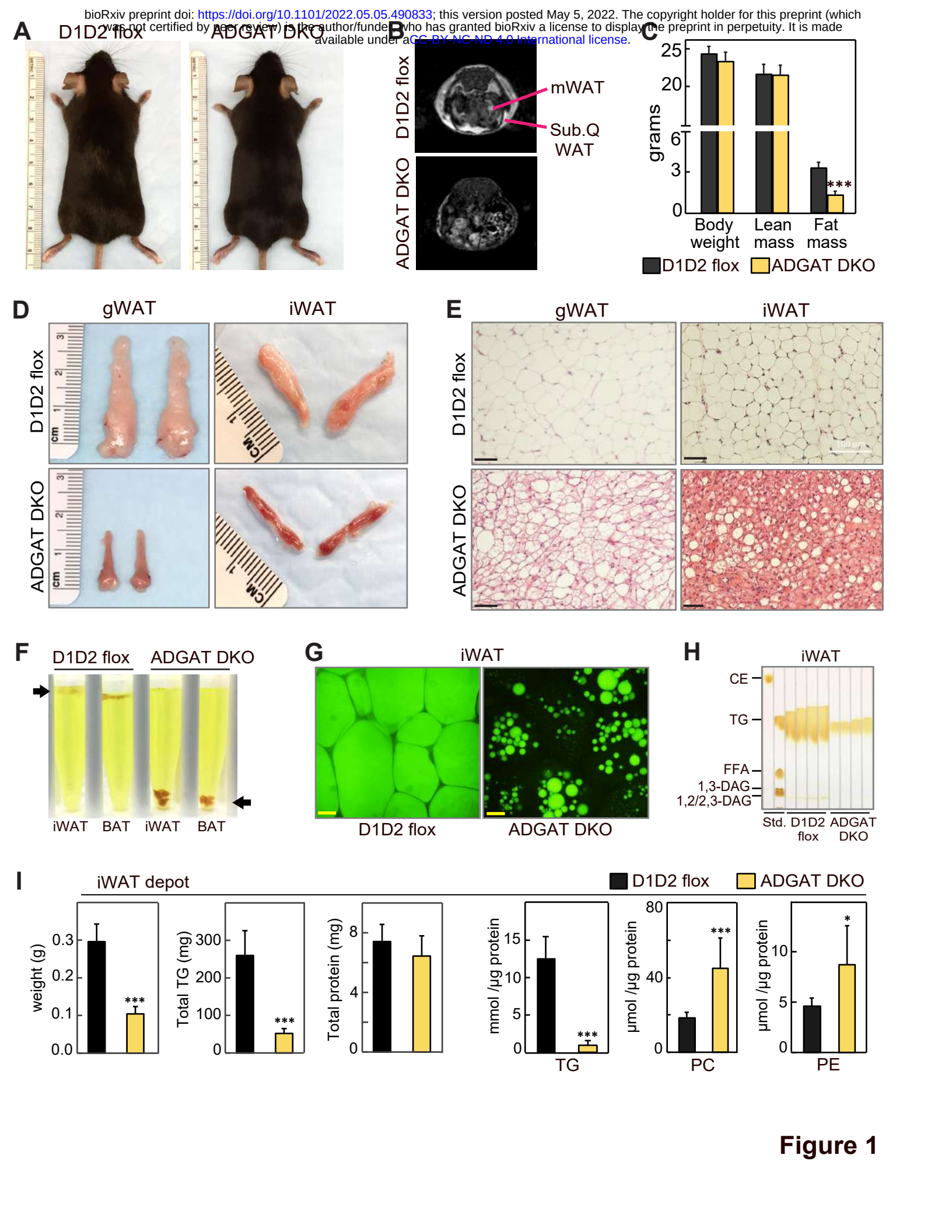

Figure 1

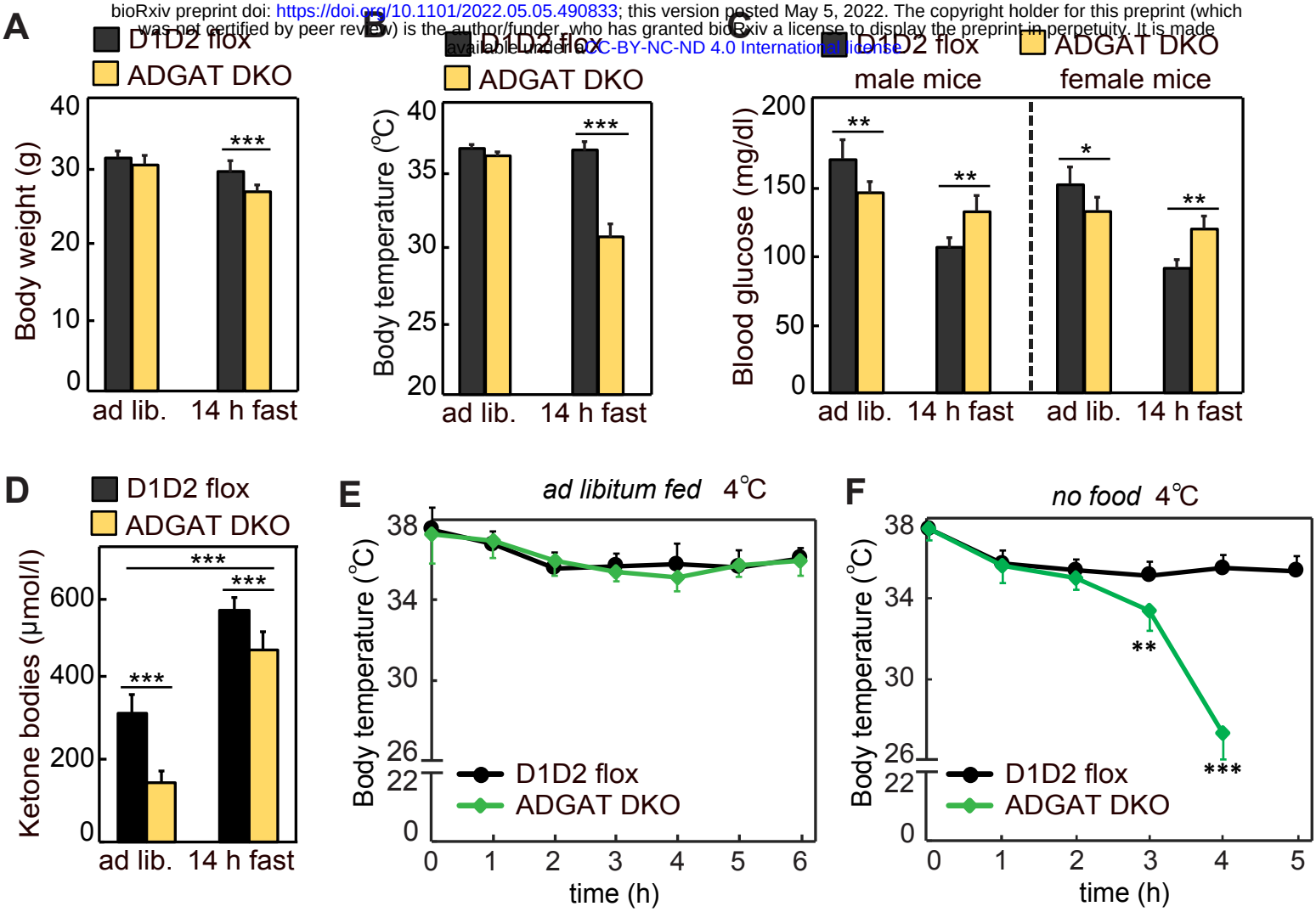

Figure 2

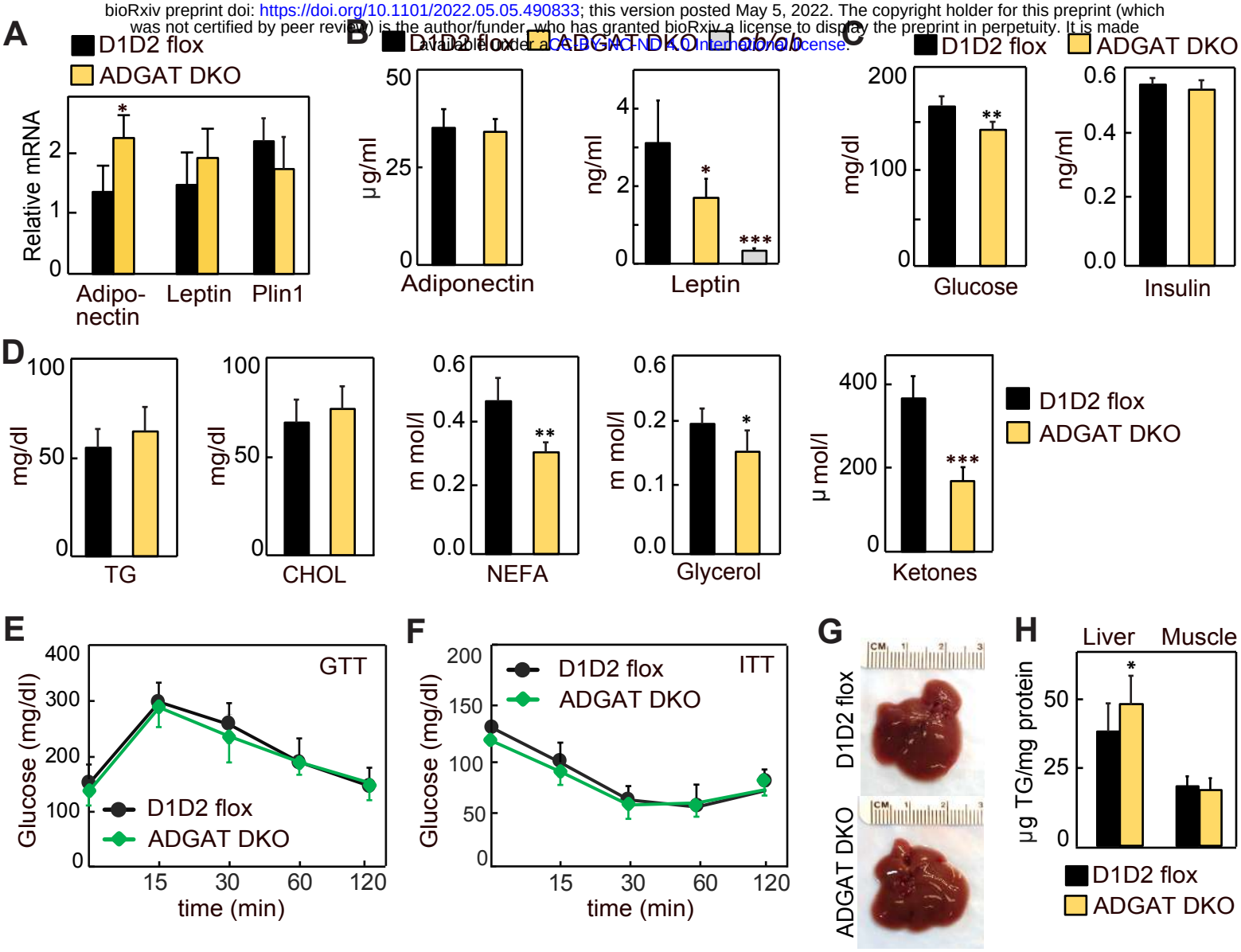

Figure 3

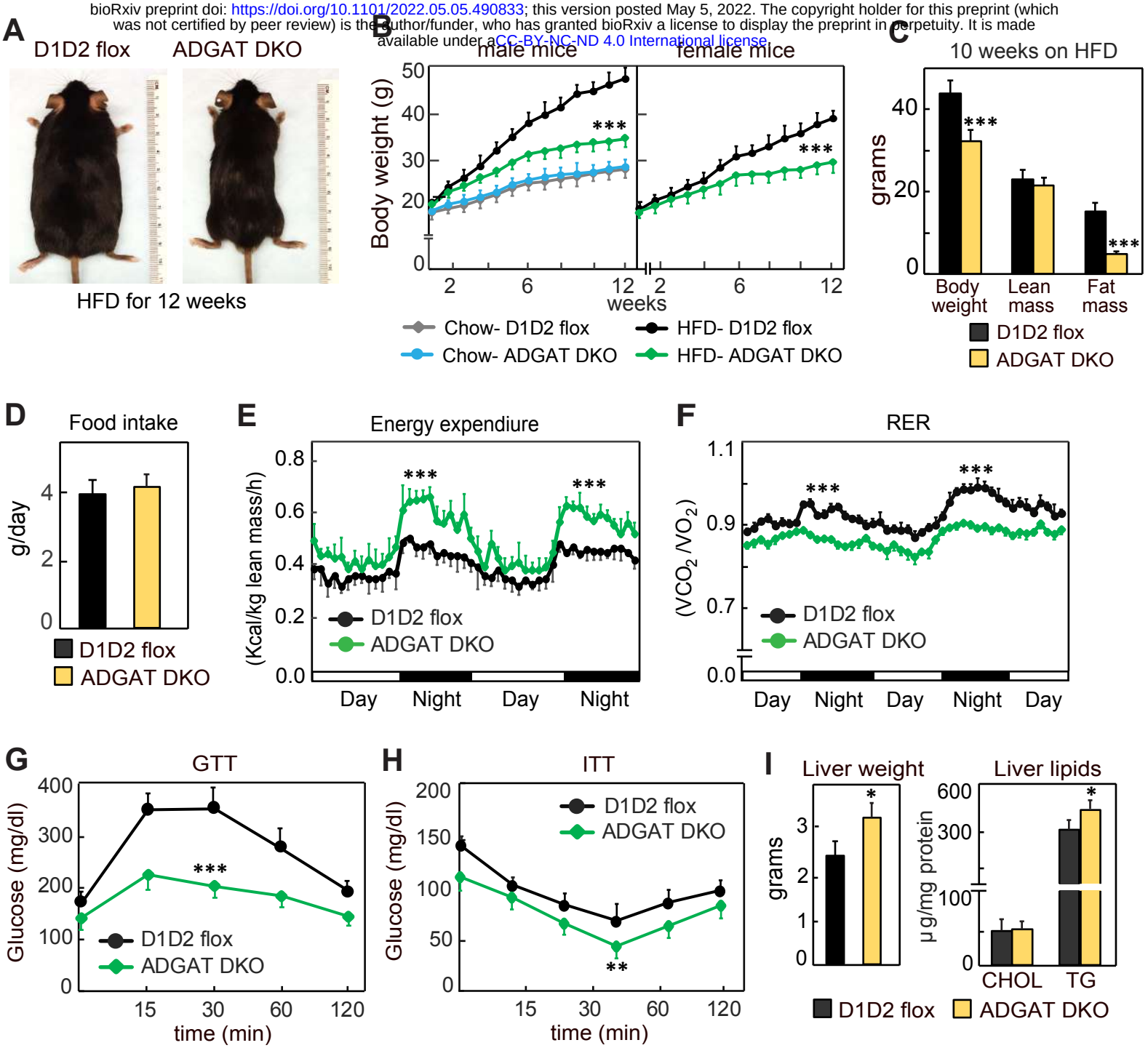

Figure 4

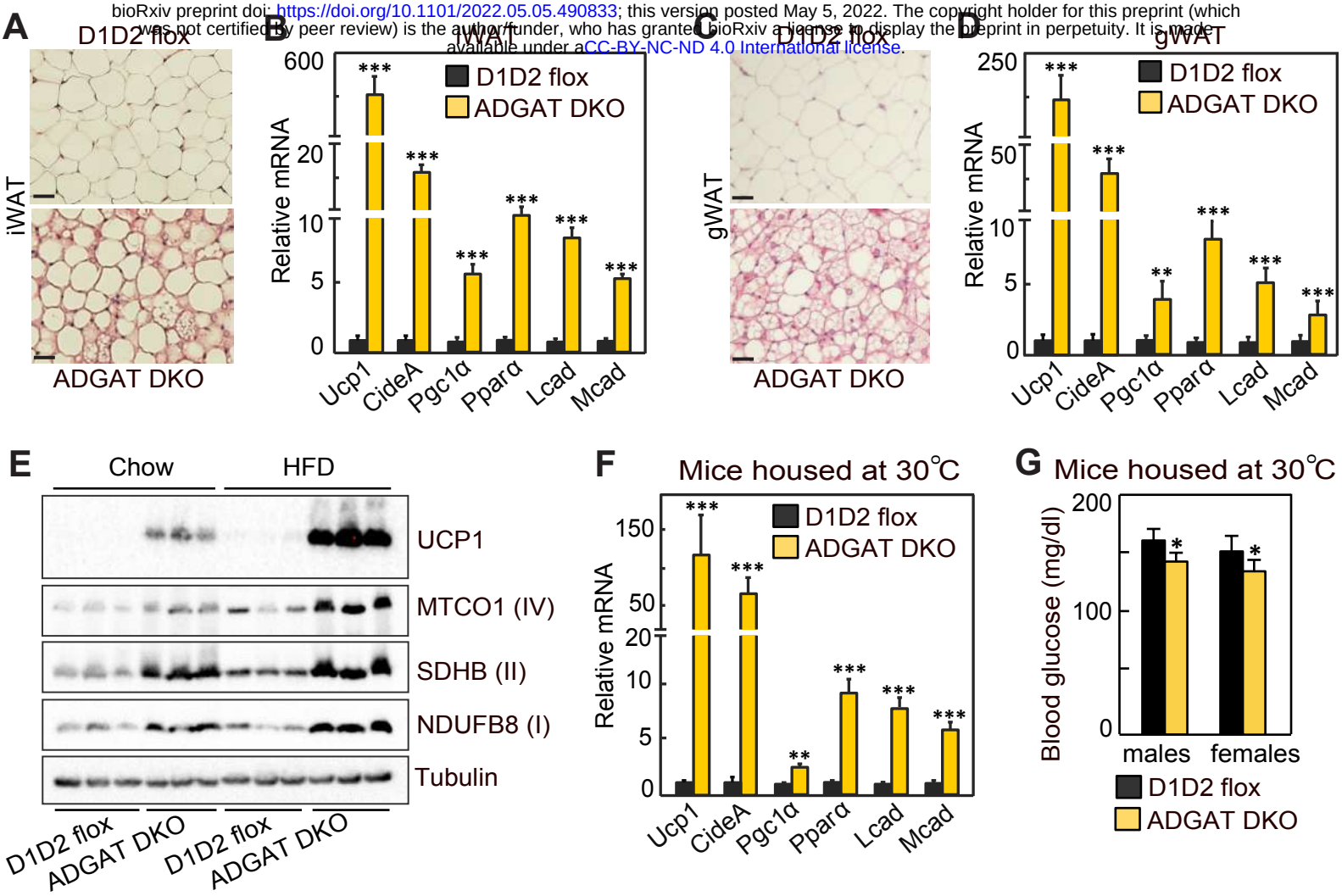

Figure 5

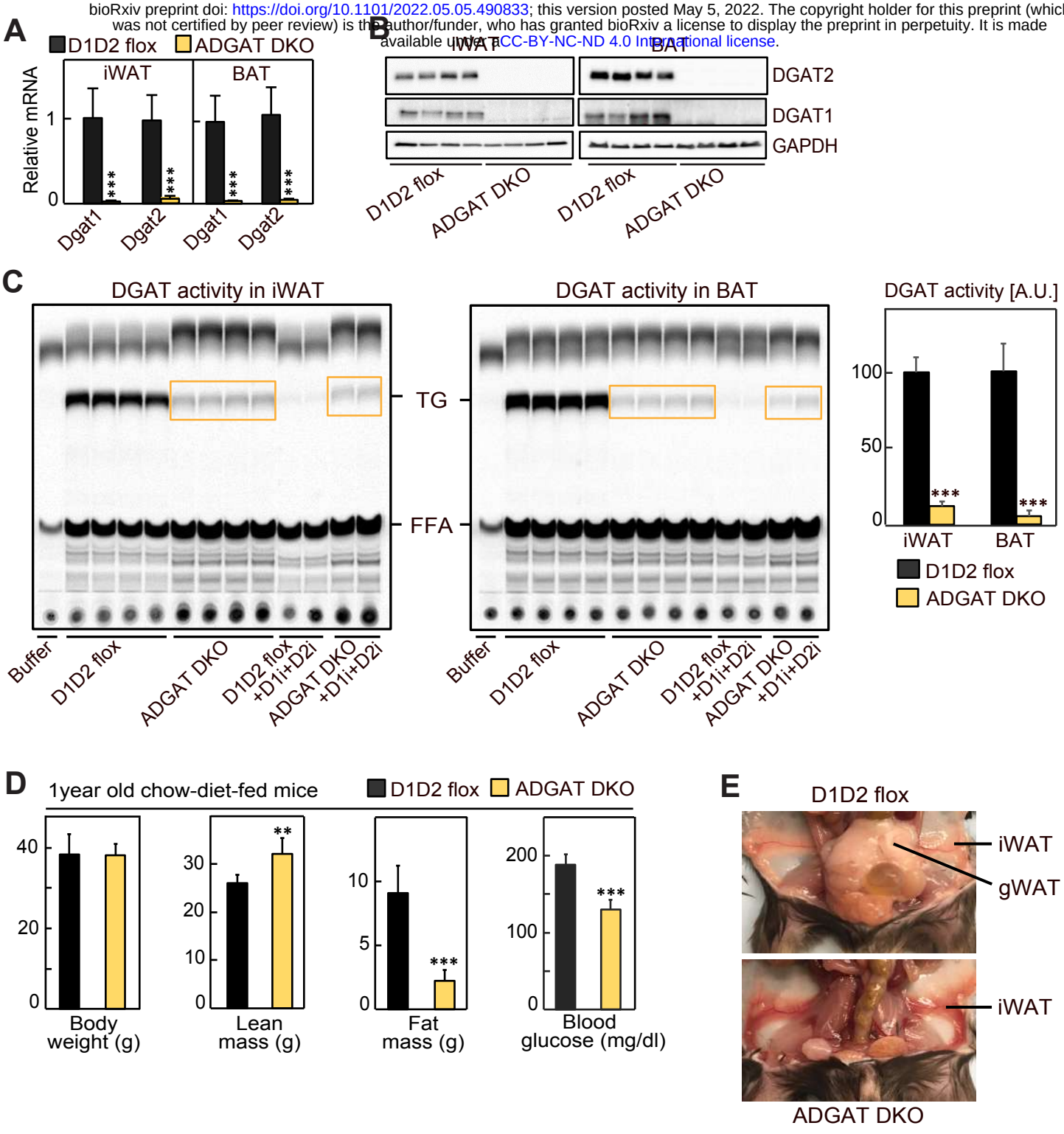

Figure S1. Related to figure 1

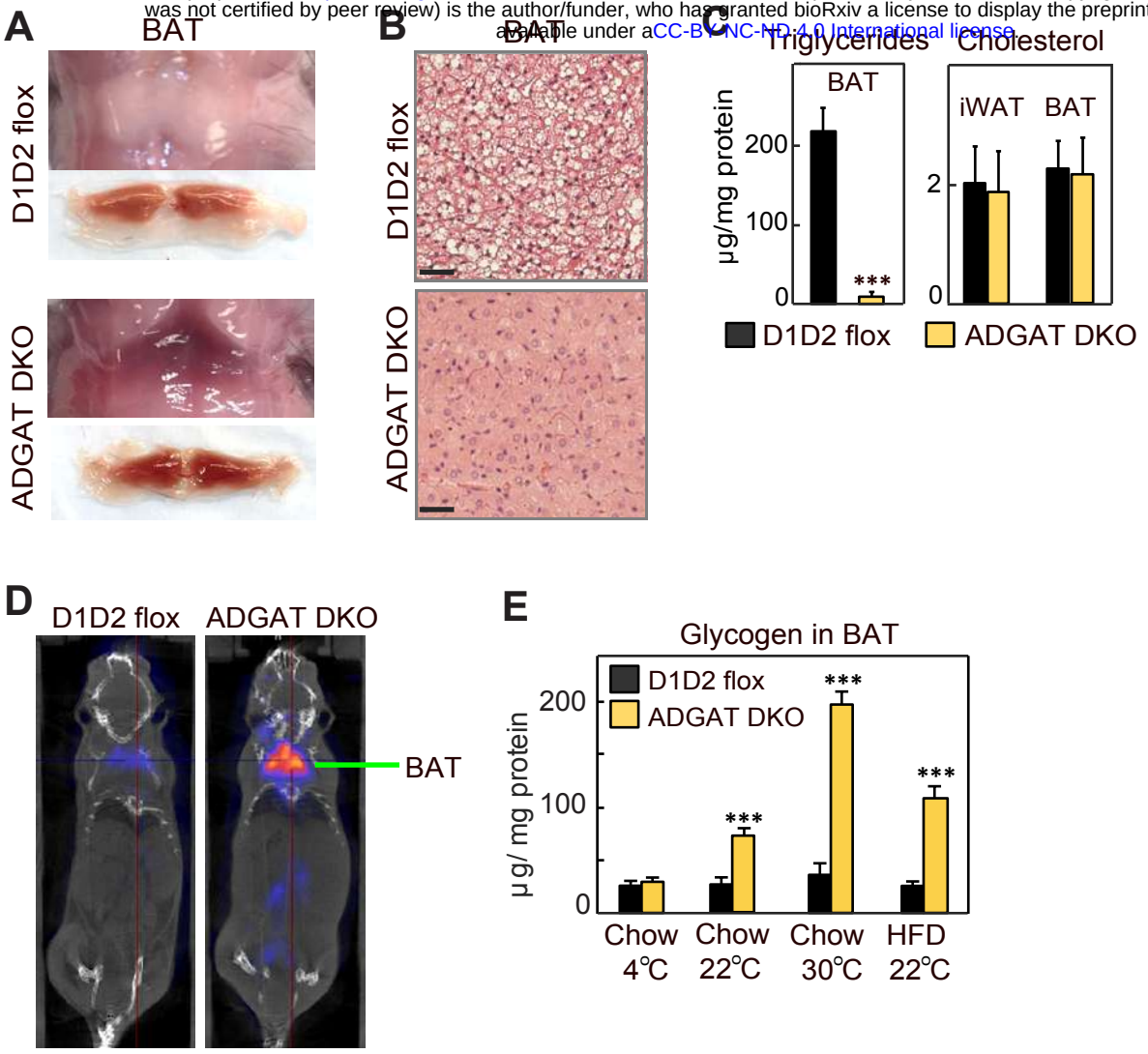

Figure S2. Related to figure 1

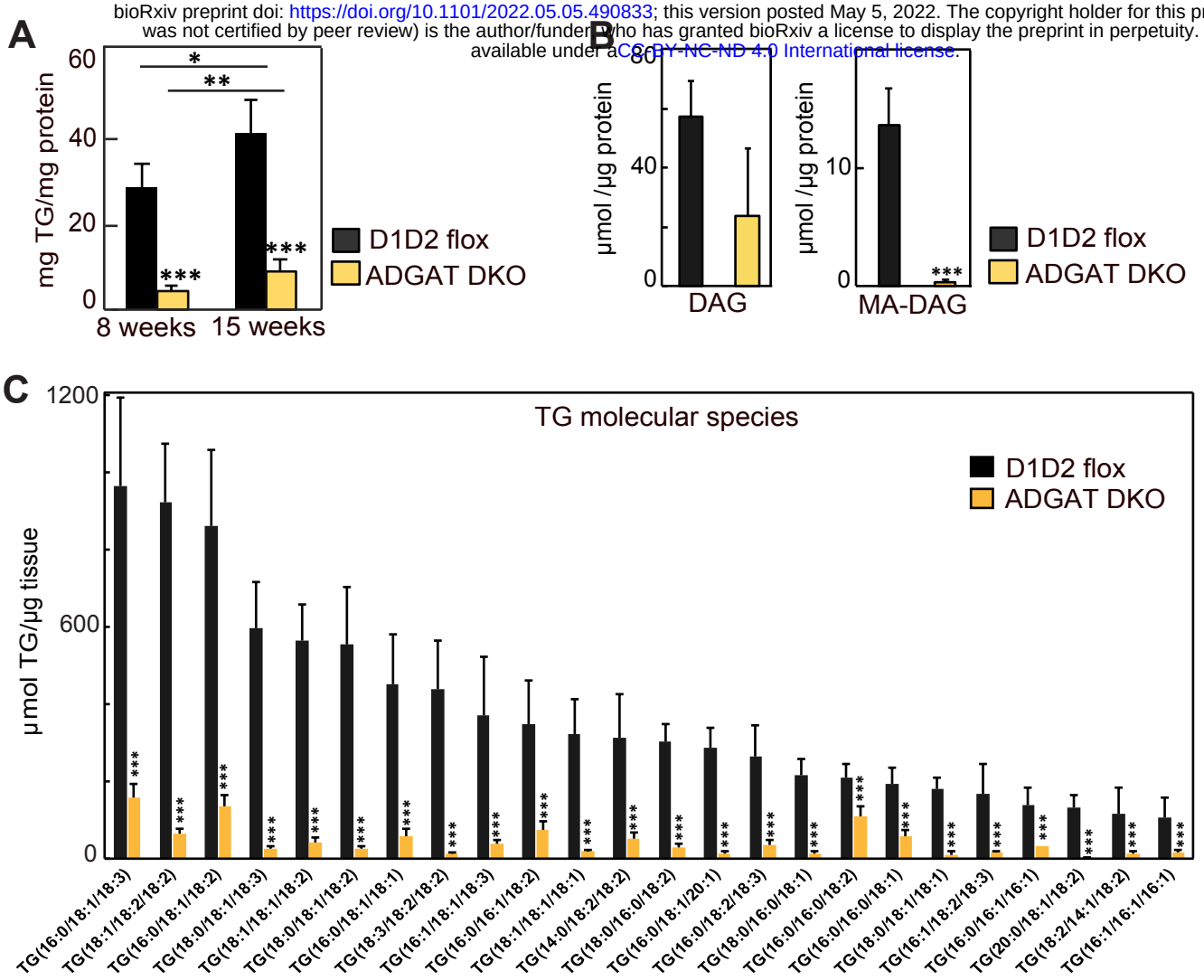

Figure S3. Related to figure 1

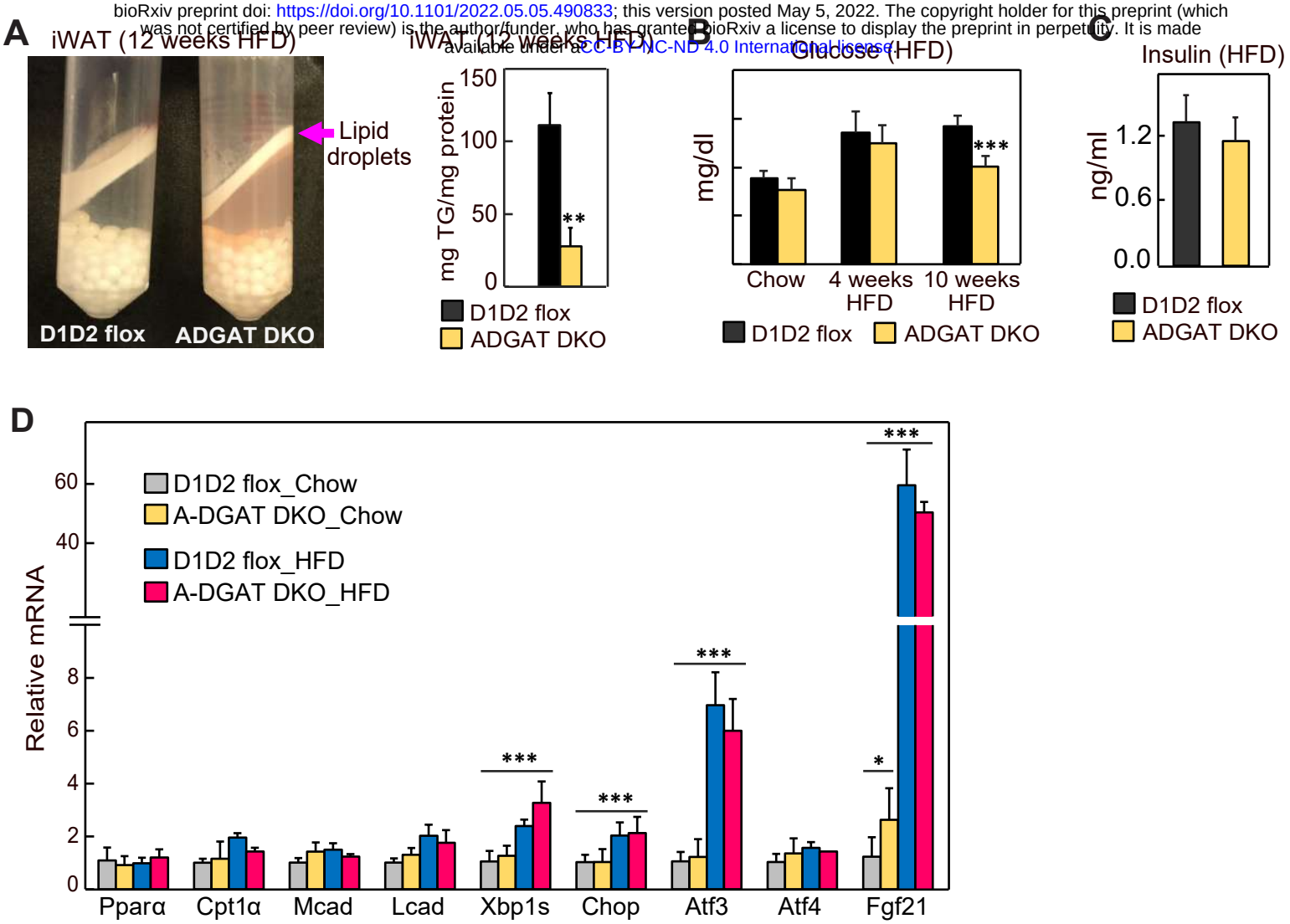

Figure S4. Related to figure 4

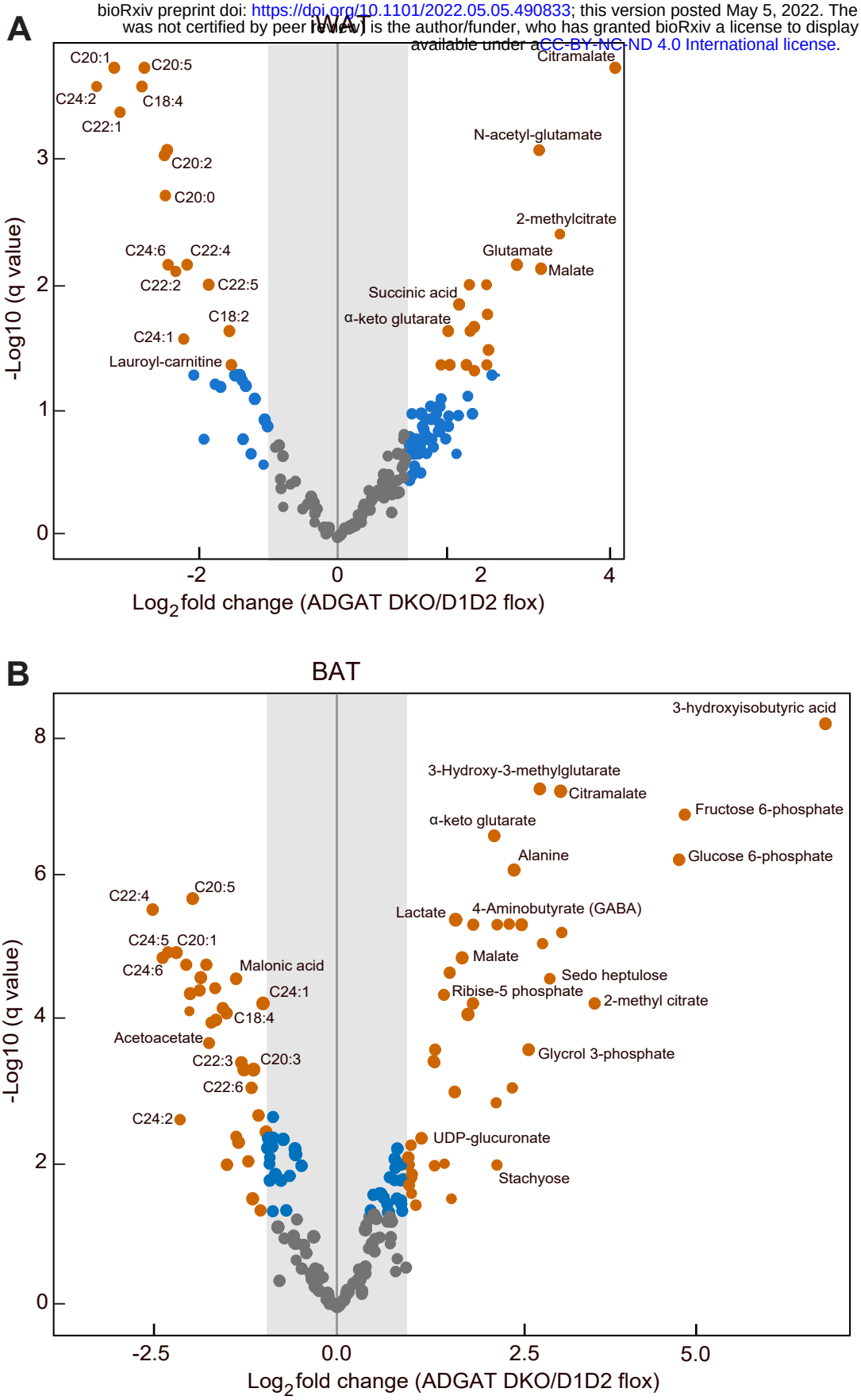

Figure S5. Related to figure 5

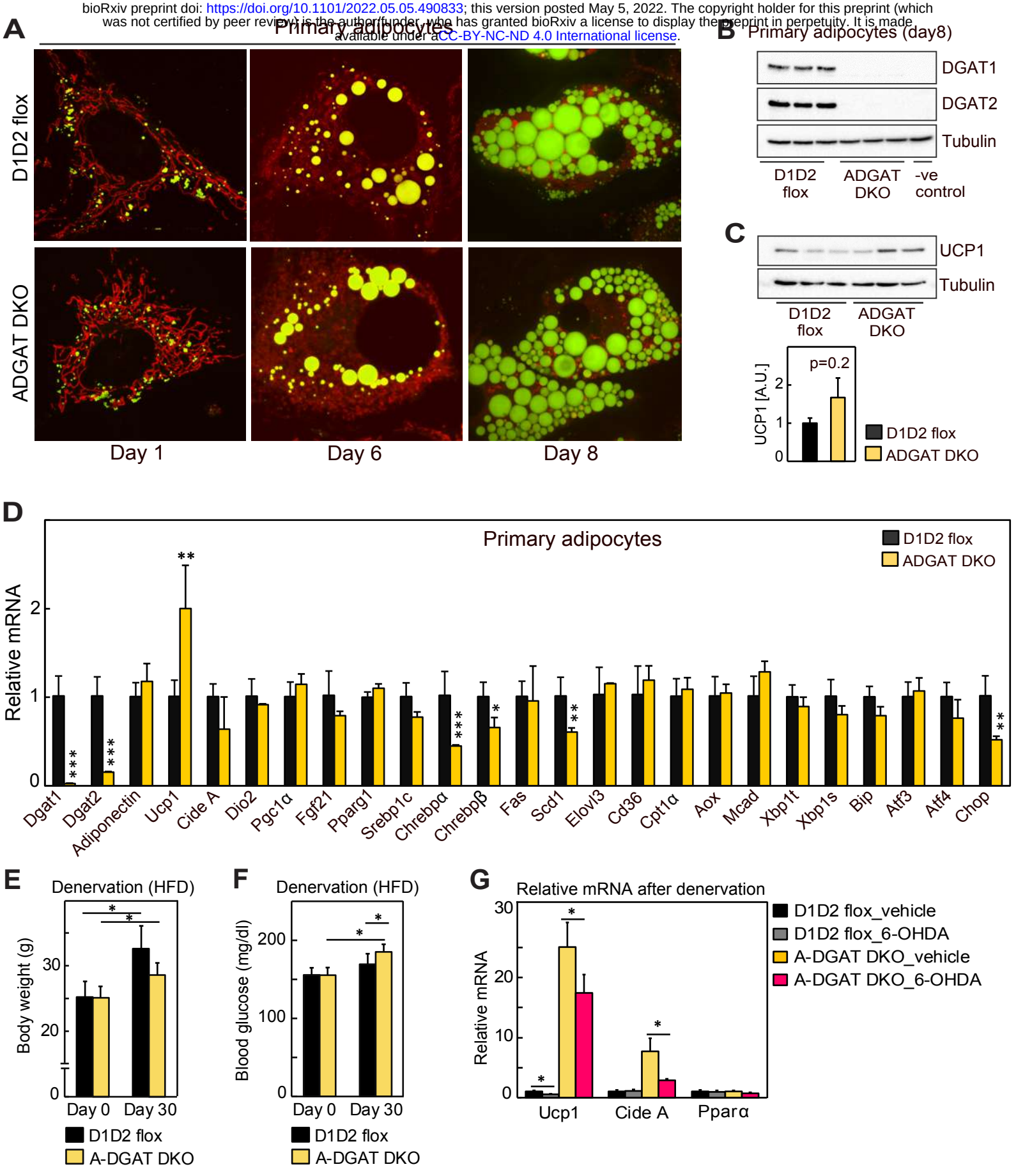

Figure S6. Related to figure 5

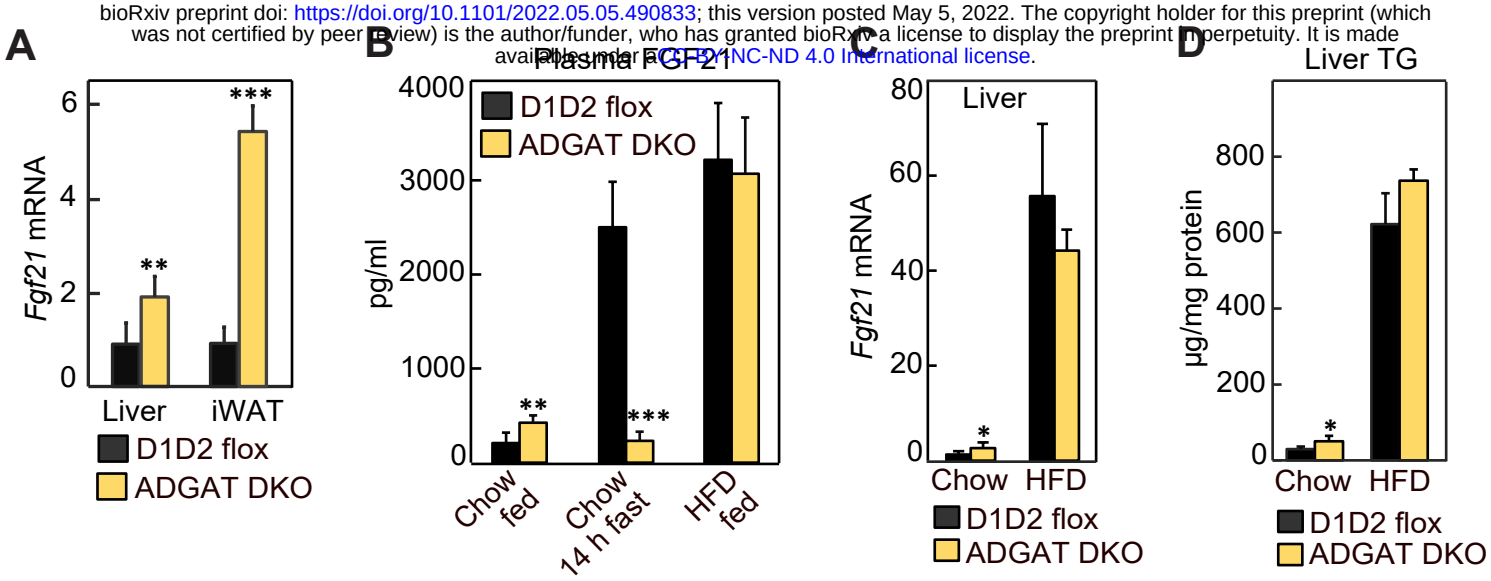

Figure S7. Related to figure 5